Annual Activity Report

on

Japan-ASEAN Science, Technology and Innovation Platform (JASTIP),

Work Package 2 (WP2)

on Energy and Environment

1st October to 30th September 2023

1.1 Development of Bio-based Carbon Materials for Energy Storage Applications

Researchers
1. Prof. Dr. Takeshi Abe Kyoto University
2. Dr. Sumittra Charojrochkul National Energy Technology Center (ENTEC), NSTDA
3. Dr. Pimpa Limthongkul National Energy Technology Center (ENTEC), NSTDA
4. Dr. Vituruch Goodwin National Energy Technology Center (ENTEC), NSTDA
5. Asst. Prof. Dr. Yuto Miyahara Kyoto University
6. Mr. Thanathon Sesuk National Energy Technology Center (ENTEC), NSTDA

Abstract

The development of bio-based carbon materials is a part of promoting the Bio Circular Green Economy (BCG) model in accordance with current Thai government policy. In this study, oil palm agricultural waste, specifically palm empty fruit bunch (PEFB) and palm shell (PS) were investigated as raw materials for producing activated carbon intended for supercapacitor applications. The primary objective was to explore the synthesis conditions and nitrogen doping effects on activated carbon derived from oil palm biomass, aiming for high-performance supercapacitors. A unique combination of chemical and surface modification processes was employed, utilizing hydrothermal process and nitrogen doping with various nitrogen sources to achieve activated carbon with a high surface area and tailored pore and surface characteristics. This research is an extension of the previous success work in producing activated carbon from palm empty fruit bunch (PEFB) and palm shell (PS), which exhibited a high capacitance level surpasses that of commercially available activated carbon in an aqueous electrolyte.
Two different nitrogen sources were employed for doping activated carbon from PEFB and PS to enhance the ion conductivity of electrode and electrolyte in supercapacitors. The impact of nitrogen addition on pore generation including both micropore and mesopore was investigated. Previous studies have indicated that nitrogen functional groups formed on activated carbon surface can facilitate electrolyte ion transportation in supercapacitors. Thus, nitrogen doping when combined with chemical activation process, has the potential to enhance the electrochemical properties of activated carbon when used as an electrode in both aqueous and organic electrolyte supercapacitors.
The activated carbon derived from PEFB and PS biomass demonstrated good properties, including high surface area and porosity. To further enhance the electrical conductivity of activated carbon, modifications of carbon surface involving nitrogen doping with ammonium chloride or urea followed by thermal activation at 800°C were explored. The effect of different nitrogen sources on electrochemical performance was reported. The modified activated carbon was evaluated in a coin cell to determine the specific capacitance using galvanostatic charge-discharge method. The nitrogen-doped PEFB activated carbon with ammonium chloride and urea, exhibited lower specific capacitance than those of undoped PEFB activated carbon (78 F g^{-1} at current loading of 0.02 A g^{-1}) in a non-aqueous 1 M $TEABF_4$/PC electrolyte. The presence of mesopores in the undoped PEFB and PS activated carbons facilitated ion transportation process, especially TEA+ and BF4- ions which have large ion radius, hence having lower internal resistance in the cell. On the contrary, modification PEFB activated carbon with ammonium chloride or urea doping reduced mesopores. During nitrogen doping process mesopores transform to micropore, hence restricting organic electrolyte ion transportation leading to higher internal resistance in the cell with N-doped PEFB activated carbon as electrode. The N-doped activated carbon derives from palm shell, PS-HWZA, displayed high specific capacitance in organic electrolyte due to its retained mesoporous structure.

Research Summary

1. Assessing the electrochemical performance of nitrogen-doped activated Carbon derived from oil palm biomass in organic electrolyte supercapacitors

Materials and Methods

Production of nitrogen-doped activated carbon derived from PEFB and PS

This study investigated the effect of different nitrogen sources doping into the activated carbon derived from oil palm biomass. All experiments utilized palm empty fruit bunch (PEFB) and palm shell (PS) as the raw materials. Hydrochar from oil palm biomass underwent hydrothermal carbonization (HTC) and was subsequently mixed with $ZnCl_2$, activating agent, and nitrogen source. Two different nitrogen sources, which are ammonium chloride, and urea were applied to generate N-doped activated carbon. The resulting mixture was activated at 800°C under CO_2 atmosphere. The nitrogen-doped activated carbon from oil palm biomass was used as electrode materials in a supercapacitor coin cell. The supercapacitor performance was evaluated using GCD test in non-aqueous electrolyte, 1 M $TEABF_4$/PC. Figure 1 depicts a schematic of the overall production process of nitrogen-doped activated carbon derived from PEFB and PS biomass.

Biobased activated carbon via hydrothermal carbonization with nitrogen doping

Figure 1 The schematic of a production process of nitrogen-doped PEFB and PS activated carbon.

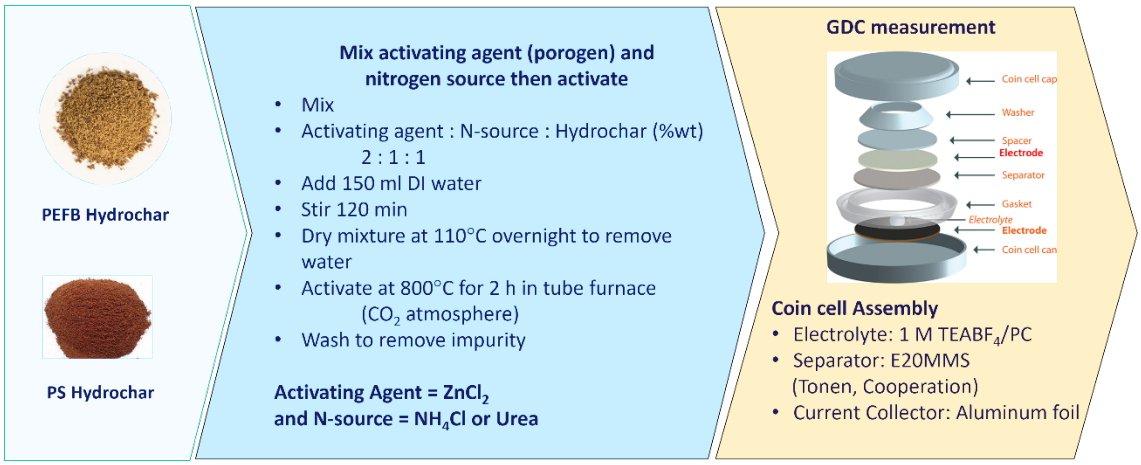

The specific capacitance value of nitrogen-doped activated carbons derived from PEFB and PS were calculated from a discharge curve of galvanostatic charge-discharge test (GCD). The electrochemical performance was assessed using the two-electrode coin cell configuration and was assembled as illustrated in Figure 2. The nitrogen-doped activated carbon and conductive carbon were dried at 80°C for at least 3 hours in a vacuum oven before use. Subsequently, the activated carbon sample and conductive carbon were mixed in a mortar with the ratio of 80:10 by weight. The carbon mixture was then transferred into the mixing container, where 12% wt. PVDF in NMP binder was added to the carbon powder mixture. The mixture was blending in a planetary centrifugal mixer at 1200 rpm for 10 minutes or until achieving a homogeneous slurry. The carbon slurry was then spread onto the aluminum foil which is serving as a current collector. The slurry was cast using a doctor blade set at a height of 80 microns. The aluminum foil coated with activated carbon was dried in a vacuum oven at 80°C for at least 12 hours. The prepared activated carbon electrode sheet was cut to a diameter of 15.8 mm with an electrode puncher. After that, the carbon electrode sheet was dried for at least 3 hours at 80°C in a vacuum oven and then allowed to cool to room temperature in a desiccator.

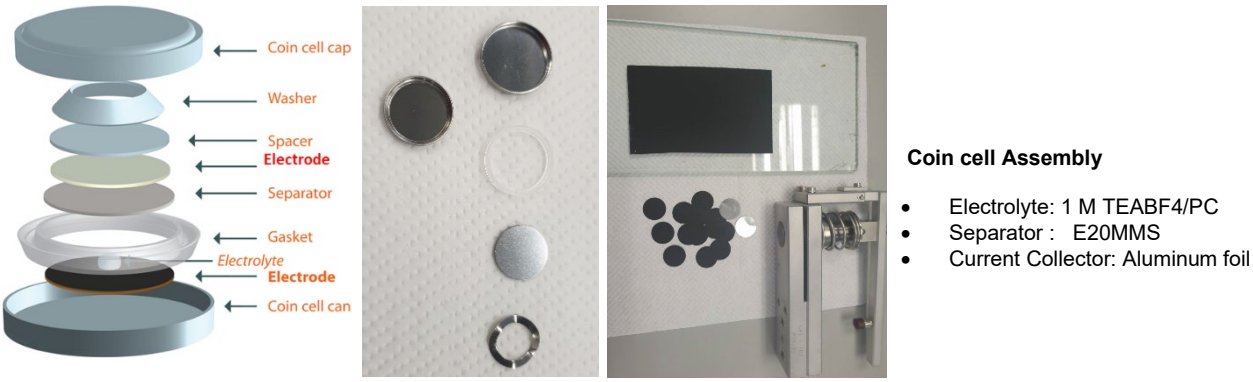

Figure 2 Coin cell assembly for electrochemical performance test of nitrogen-doped activated carbon derived from PEFB and PS

Characterization method and electrochemical test of activated carbon derived from PEFB

The surface area and pore size distribution of activated carbon (AC) samples were analyzed using nitrogen adsorption-desorption technique and Brunauer–Emmett–Teller (BET) theory, conducting using Micromeritics ASAP 2460 instrument. Pore volume and pore size distribution (PSD) were determined employing non-local density functional theory (NLDFT). Galvanostatic charge-discharge test (GCD) was conducted on supercapacitor coin cell using constant current charge-discharge method. The GCD rate performance was carried out at various current density using MACCOR machine, where the charge and discharge rates were set at the current densities of 0.02, 0.05, 0.1, 0.2, 0.5 and 1 A g^{-1}, 10 cycles at first rate and then 5 cycle each following rate. The voltage range is set at 0 – 2.5 V to measure the capacitance of the carbon electrode in non-aqueous electrolyte, 1 M $TEABF_4$/PC. Electrochemical impedance spectroscopy (EIS) measurement was carried out over the frequency range of 10^{-2} – 10^5 Hz with a signal amplitude of 10 mV. EIS measurement was conducted using an Autolab PGSTAT204 potentiostat/galvanostat instrument.

Results and discussion

The specific surface area and pore properties of nitrogen-doped PEFB activated carbon

The pore size distribution plot of nitrogen-doped PEFB activated carbons are displayed in Figure 3 (a). All nitrogen-doped activated carbons have high surface area which contained mostly micropore (<2 nm). As shown in Figure 3 (a), the pore size distribution plot reveals differences between activated carbon without nitrogen doping (EFB-HWZ-800) and those activated carbon samples doped with ammonium chloride or urea (EFB-HWZA-800 and EFB-HWZU-800, respectively). It can be clearly seen that activated carbon without nitrogen doping exhibits a notably higher mesopore volume compared to nitrogen-doped activated carbons. The undoped activated carbon has a lower surface area of 1599 m^2 g^{-1}, while nitrogen-doped activated carbons, HWZA and HWZU have surface area of 1650 and 1634 m^2 g^{-1}, respectively. It was found that when the activating temperature was increased, the microporous volume of activated carbon was also increased. The results of specific surface area (BET) and pore volume are shown in Table 1.
Figure 3 (b) shows the nitrogen gas adsorption and desorption isotherms of highly porous materials. The isotherm of the undoped activated carbon surpasses that of the nitrogen-doped carbons, owing to the larger pore size of the former. This isotherm plot also shows that activated carbon without nitrogen addition has a hysteresis loop in the form of Type H2, which shows the type of ink-bottle-shaped pores found in activated carbon with high amounts of mesopores. Consequently, a greater quantity of nitrogen gas absorption is observed in the latter stage.

Nitrogen-doped activated carbons, on the other hand, display a hysteresis loop characteristic of H4 slit-shaped pores. This structure is typical for activated carbon containing high amounts of micropores. The slip shape micropore could facilitate and enhance movement are enhanced movement of charges from the electrolyte in the case that the ion size and pore size are comparable.

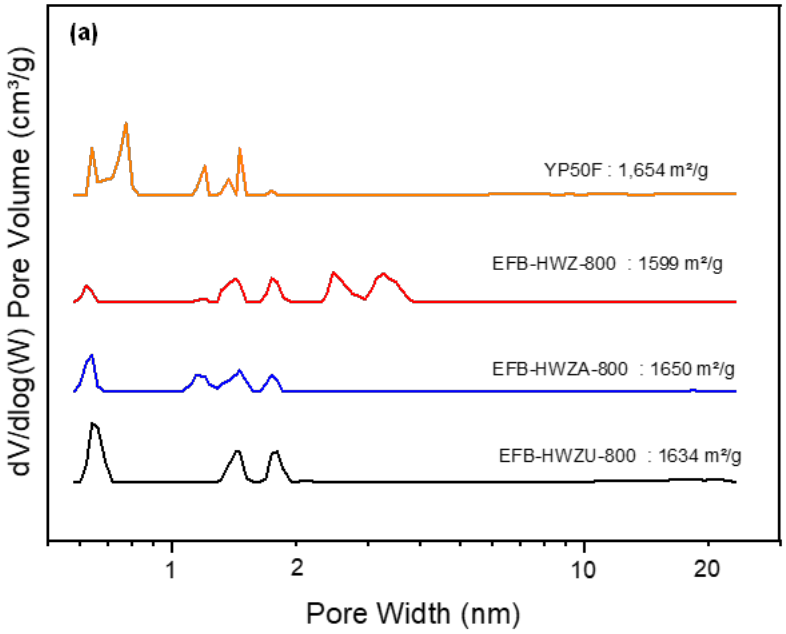

Figure 3 (a) Pore size distribution plot of undoped activated carbon (EFB-HWZ-800), NH_4Cl-doped activated carbon (EFB-HWZA-800), Urea-doped activated carbon (EFB-HWZU-800) and commercial carbon (YP50F)

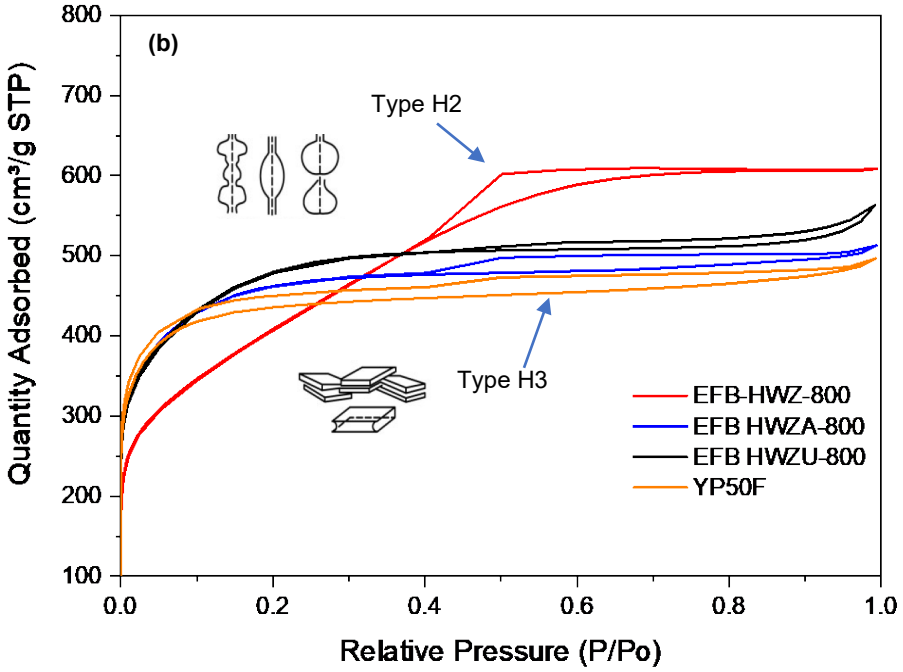

Figure 3 (b) Nitrogen adsorption-desorption isotherms of undoped activated carbon (EFB-HWZ-800), NH_4Cl-doped activated carbon (EFB-HWZA-800), Urea-doped activated carbon (EFB-HWZU-800) and commercial carbon (YP50F)

Table 1. BET surface area and pore volume of nitrogen-doped PEFB activated carbons and YP-50F (commercial carbon)

Activated Carbon	**BET surface area** ($m^2\ g^{-1}$)	**Cumulative Volume** ($cm^3\ g^{-1}$)		Mesopore (%)
		Micropore	Mesopore	
EFB-HWZ-800	1599	0.52	0.72	57.78
EFB-HWZA-800	1650	0.66	0.06	4.07
EFB-HWZU-800	1634	0.69	0.08	10.08
YP50F	1654	0.65	0.05	7.96

From Table 1, both activated carbon samples doped with ammonium chloride and urea exhibit high values of micropore volume between 0.66 to 0.69 $cm^3\ g^{-1}$. As illustrated in Figure 3 (a), the nitrogen-doped activated carbons contain the majority of micropores which have pore size approximately between 0.6 to 0.7 nm. The pore diameter of 0.6 to 0.7 nm was found to be effectively suitable to accommodate the ion in aqueous electrolyte system. However, for non-aqueous electrolyte which has larger ion size, the combination of micro and mesopore in the undoped PEFB activated carbon has shown to enhance ion transportation more than the nitrogen-doped activated carbon.

The specific capacitance from galvanostatic charge-discharge test (GCD) of nitrogen-doped PEFB activated carbon

The capacitance values of nitrogen-doped PEFB activated carbon are shown in Figure 4. This figure compares the capacitance of nitrogen-doped activated carbons, synthesized with NH_4Cl or urea as nitrogen source added on hydrochar and activated with $ZnCl_2$ at 800°C with the undoped PEFB activated carbon and YP50F commercial carbon. It was observed that the biobased activated carbon, undoped and nitrogen-doped from either NH_4Cl or urea, all samples exhibit higher specific capacitance values at 0.02 A g^{-1} current density from GCD tests compared to the commercial carbon, YP-50F. This promising result demonstrates that the biobased PEFB activated carbon has a high potential for as an electrode material for high performance supercapacitors.
The effect of nitrogen doping with NH4Cl or urea on PEFB hydrochar has significantly lower the capacitance values when testing at high current density. As the current density increases, the mobility of ion moving toward the pore surface is higher, hence the large ion in non-aqueous electrolyte could be obstructed from entering the micropores. There is a possibility of a detrimental effect that is caused by the addition of nitrogen atom which could block or narrow the pore size of the nitrogen-doped activated carbon. Both ammonium chloride and urea doped activated carbon cannot retain their high capacitance value with increasing current density charging rate. Only undoped PEFB activated carbon can exhibit higher capacitance value compared to commercial carbon when tested at 1 A g^{-1}. Thus, the existence of mesopores in the undoped PEFB activated carbon has played an important role to enhance the capacitance of supercapacitor with non-aqueous electrolyte.

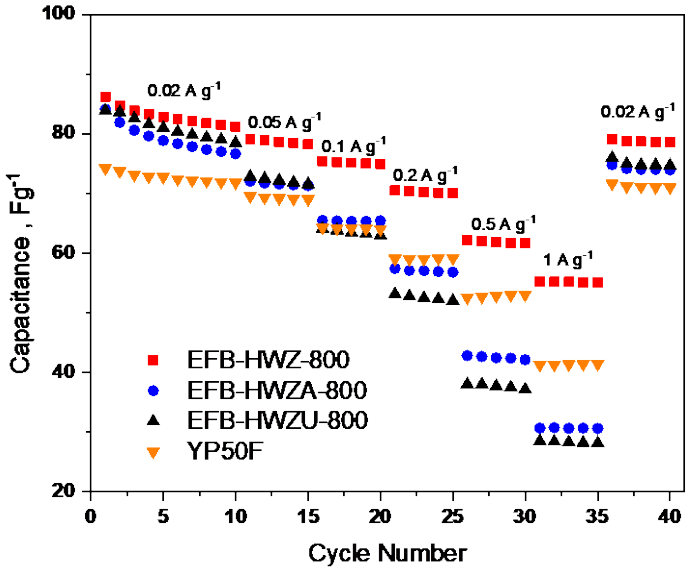

Figure 4 Specific capacitance from GCD test of undoped PEFB activated carbon (HWZ-800) nitrogen-doped PEFB activated carbon, doping with NH_4Cl (HWZA-800), doping with urea (HWZU-800) and YP50F commercial carbon as a benchmark

The Electrochemical Impedance Spectroscopy (EIS) results of nitrogen-doped PEFB activated carbon

The Nyquist plot results obtained from EIS experiments conducted on both undoped and nitrogen-doped activated carbon derived from PEFB are presented in Figure 5. Analysis of the EIS results reveal that the undoped activated carbon, designated as HWZ, exhibits a lower internal resistance compared to nitrogen-doped activated carbon, HWZA and HWZU. This low value in internal resistance is attributed to the less resistance in ion diffusion from electrolyte to porous carbon electrode. Conversely, the high internal resistance observed in nitrogen-doped activated carbon may be caused from the decreased of mesopore, which play a crucial role in facilitating the transportation of large organic ions in non-aqueous electrolytes. Consequently, there are more constraints on ion transportation into micropore within nitrogen-doped activated carbon.

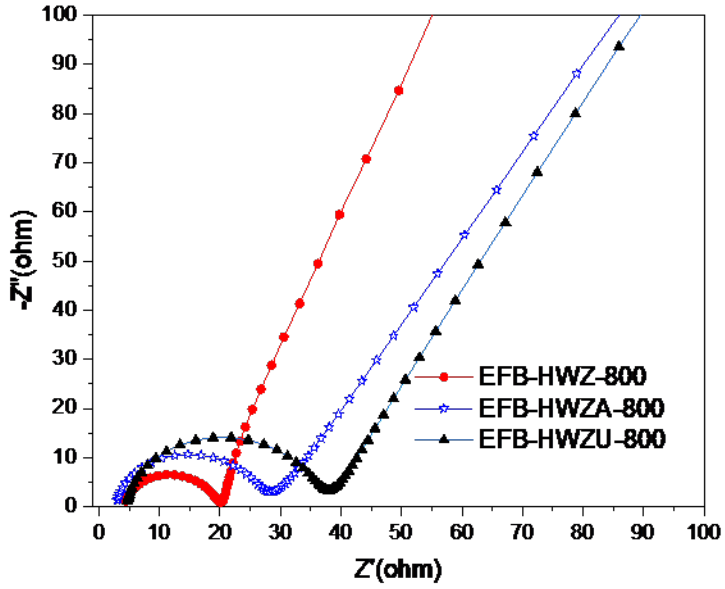

Figure 5 Nyquist plot results from EIS of both undoped, HWZ, and nitrogen-doped activated carbon derived from PEFB, HWZA and HWZU

Conclusion

The effect of nitrogen doping during activation process was investigated using palm empty fruit bunches (PEFB) as the starting biomass. It was found that nitrogen doping during the activation process did not show significant effect on the surface area. However, the addition of nitrogen affected the formation of mesopore in activated carbon. For undoped PEFB activated carbon, the higher activation temperature of 800°C resulted in an activated carbon with high mesopore volume. The specific capacitance of undoped activated carbon in this study is slightly higher than that of nitrogen-doped activated carbon. The NH_4Cl and urea doped PEFB activated carbon could retain high capacitance only at 0.02 A g^{-1}. The high capacitance value with increasing current density of HWZ indicates that PEFB activated carbon has good rate capability. In conclusion, both nitrogen-doped activated carbons yielded high specific capacitance at 73.9 and 74.7 F g^{-1} at 0.02 A g^{-1}, the PEFB undoped carbon reported capacitance of 79.1 F g^{-1}which are higher than YP50F at 71 F g^{-1}.

Production of nitrogen-doped palm shell (PS) activated carbon

In this section, the activated carbon was synthesized from palm shell (PS) biomass, characterized and electrochemical performance tested. The testing conditions and preparation steps for

activated carbon derived from palm shell (PS) is the same as outlined earlier for the activated carbon prepared from empty palm fruit bunches (PEFB). Three activated carbon samples derived from PS are designated as follows; PS-HWZ 800 synthesized without nitrogen doping, using $ZnCl_2$: hydrochar at weight ratio of 2:1 and activated at 800°C. PS-HWZA 800 was prepared using nitrogen doping with ammonium chloride in the activation step. The weight ratio of NH_4Cl : $ZnCl_2$: hydrochar is 1:2:1 and activated at 800°C. Finally, PS-HWZU 800 was produced using urea as nitrogen source. The urea : activating agent, $ZnCl_2$ to hydrochar ration is 1:2:1 and activated at 800°C.

The specific surface area and pore properties of nitrogen-doped PS activated carbon

The results of the specific surface area and porosity are summarized in Table 2. Surface area analysis reveals that the undoped PS activated carbon exhibits a lower specific surface area at 1487 m^2 g^{-1} compared to the ammonium chloride doped PS activated carbon which has surface area of 1641 m^2 g^{-1}. Furthermore, when examining mesopore content of PS derived activated carbon, it was found that PS activated carbon doped with ammonium chloride possesses a higher mesopore content compared to the PS activated carbon doped with urea. This discrepancy suggests that the larger molecular size of urea obstructs mesopore generation process. The pore size distribution of the nitrogen-doped PS activated carbons is depicted in Figure 6 (a).

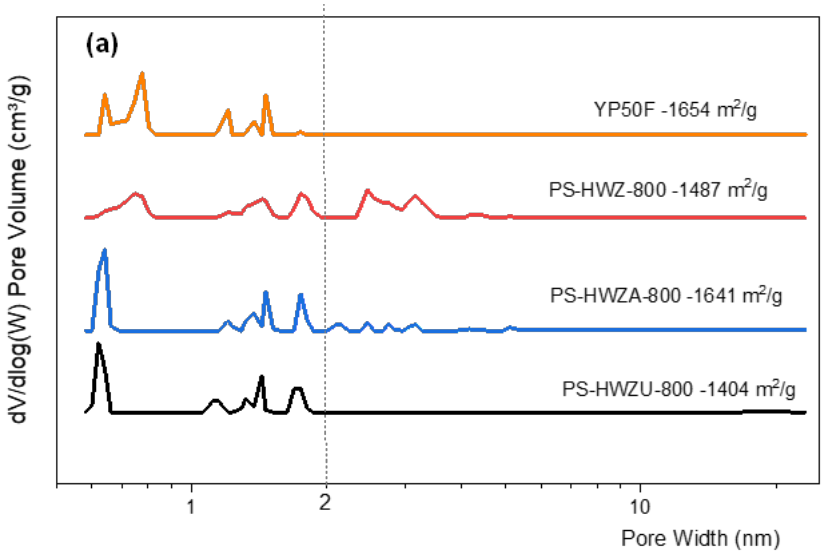

Figure 6 (a) Pore size distribution plot of commercial carbon, YP50F compared to undoped PS activated carbon, PS-HWZ-800, nitrogen-doped activated carbons using NH_4Cl as nitrogen source, PS-HWZA-800 and nitrogen-doped activated carbons using urea as nitrogen source, PS-HWZA-800

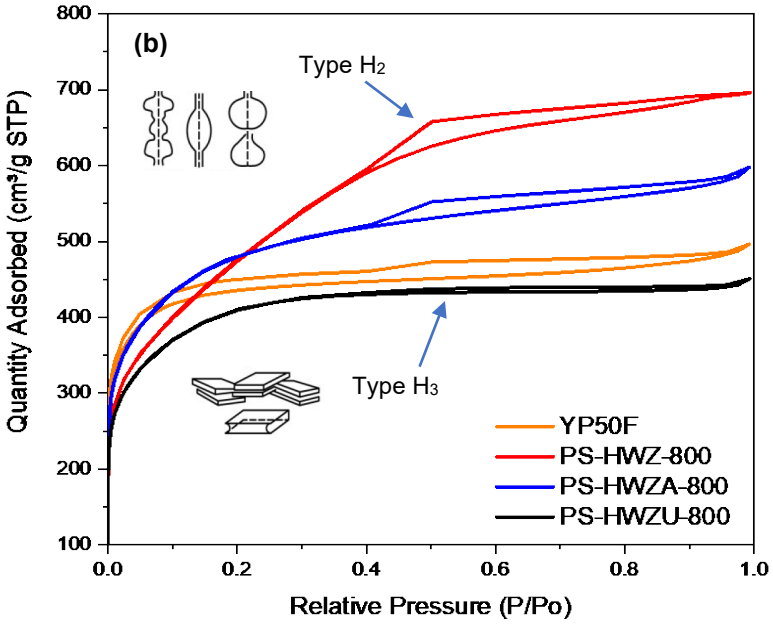

Figure 6 (b) Nitrogen adsorption-desorption isotherms of commercial carbon, YP50F compared to undoped PS activated carbon, PS-HWZ-800, nitrogen-doped activated carbons using NH_4Cl as nitrogen source, PS-HWZA-800 and nitrogen-doped activated carbons using urea as nitrogen source, PS-HWZA-800

Table 2. BET surface area and pore volume of PS derived activated carbons and YP-50F.

Activated Carbon	BET surface area ($m^2\ g^{-1}$)	Cumulative Volume ($cm^3\ g^{-1}$)		Mesopore (%)
		Micropore	Mesopore	
PS-HWZ-800	1487	0.56	0.45	44.65
PS-HWZA-800	1641	0.66	0.18	21.07
PS-HWZU-800	1404	0.61	0.01	1.82
YP50F	1654	0.65	0.05	7.96

Figure 6 (b) shows the nitrogen gas adsorption and desorption isotherms of PS derived activated carbon synthesized in this study. The isotherm of the undoped PS activated carbon and NH_4Cl doped PS activated carbon surpasses that of comer carbon, owing to the larger mesopore content of the carbon samples. Both undoped PS activated carbon and NH_4Cl doped PS activated carbon isotherms reveal that the samples have a ink-bottle-shaped pores conformed to the hysteresis loop type H2, which is found in activated carbon with high amounts of mesopores. Consequently, a greater quantity of nitrogen gas absorption is observed in the latter stage. As tabulated in Table 2, the undoped PS activated carbon has 44.65% of mesopore and NH_4Cl doped PS activated carbon has 21.07% of mesopore.

Electrochemical test, GCD result of nitrogen-doped PS Activated Carbon

The Galvanostatic Charge-Discharge (GCD) test results of PS activated carbons are illustrated in Figure 7. It can be seen that the nitrogen-doped PS activated carbons (PS-HWZA-800) demonstrates higher specific capacitance than the undoped activated carbon (PS-HWZ-800).

Additionally, when compared to the commercial carbon, YP-50F, PS-HWZU-800 exhibits higher capacitance at a current density of 1 A g^{-1}. The effect of urea doping (PS-HWZU-800) is also observed in this case. However, PS-HWZU-800 activated carbon experiences a consistent decrease in capacitance during charge at high current density (0.2 to 1 A g^{-1}), potentially attributed to the low mesoporous structure of the samples. Whereas with commercial carbon, YP50F displays the largest decrease in capacitance with increasing current density, indicated that commercial carbon which contains most of the microporous structure affect the rate capability of the supercapacitor with non-aqueous electrolyte. The undoped PS activated carbon capacitance result exhibits a good rate capability of carbon electrode which is the same behavior found in NH_4Cl doped PS activated carbon.
The capacitance values of nitrogen-doped activated carbons synthesized with different nitrogen sources added onto hydrochar were compared. The undoped PS activated carbon and NH_4Cl doped PS activated carbon and urea doped PS activated carbon exhibit lower specific capacitance value than the commercial carbon, YP50F at 0.02 A.g^{-1} current density. However, at a high current density of 1 A.g^{-1} both undoped and nitrogen-doped activated carbons from NH_4Cl demonstrated higher specific capacitance values than YP50F. This promising preliminary outcome of NH_4Cl doped PS activated carbon suggests that the proportion of mesopores facilitates efficient ion transfer, leading to enhanced capacitance.

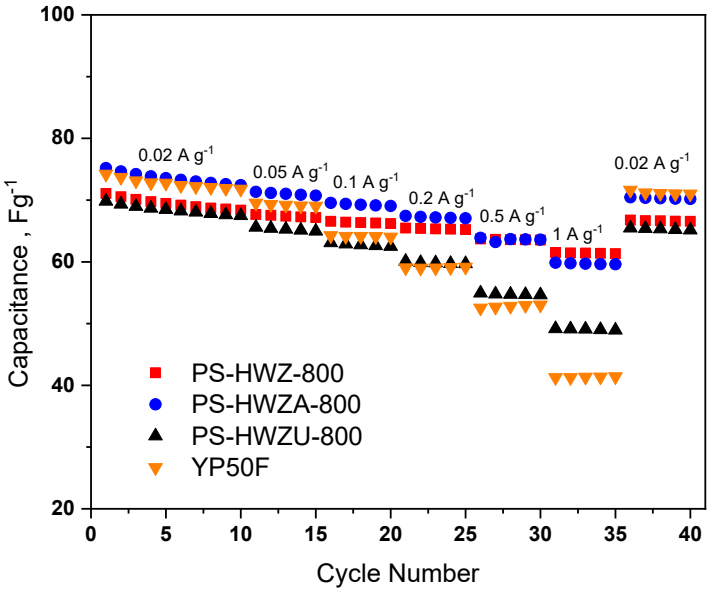

Figure 7 Specific capacitance from GCD tests of undoped PS activated carbon, PS-HWZ-800, NH_4Cl doped PS activated carbon, PS-HMZA and urea as nitrogen sources and YP50F commercial activated carbon as a benchmark

The Electrochemical Impedance Spectroscopy (EIS) results of nitrogen-doped PEFB activated carbon

The Nyquist plot results obtained from EIS experiments conducted on both undoped and nitrogen-doped activated carbon derived from PS are presented in Figure 8. The undoped PS activated carbon, designated as PS-HWZ exhibits the lowest internal resistance compared to nitrogen-doped PS activated carbon, PS-HWZA and PS-HWZU. This low value in internal resistance is attributed to the less resistance in ion diffusion resulting from high mesoporous content in the

undoped PS activated carbon. The EIS test results confirm that the amount of mesopore presents in the activated carbon plays a crucial role in facilitating the transportation of large organic ions in non-aqueous electrolytes.

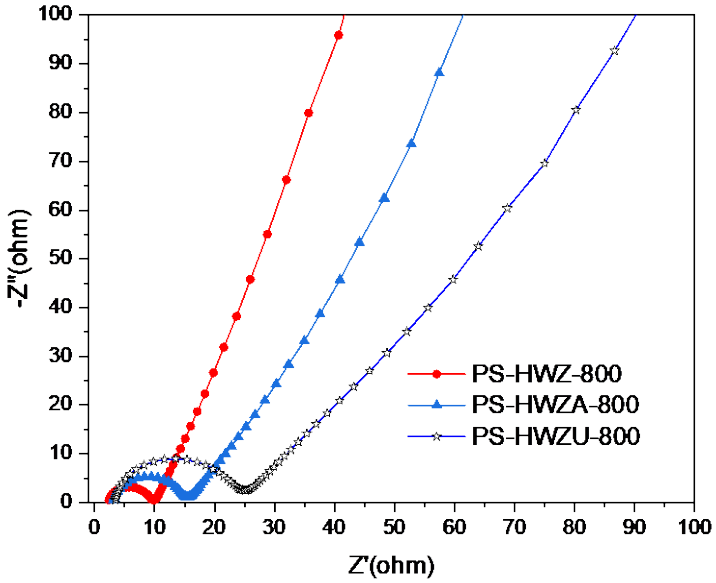

Figure 8 Nyquist plot results from EIS of both undoped, PS-HWZ, and nitrogen-doped activated carbon derived from PS, PS-HWZA and PS-HWZU

Conclusion

Activated carbon production from palm shell (PS) and palm empty fruit bunch (PEFB) biomass, along with nitrogen doping using ammonium chloride or urea, was successfully accomplished. Hydrothermal carbonization of palm empty fruit bunch (PEFB) and palm shell (PS) followed by activation using $ZnCl_2$ resulted in the production of high-surface-area and high mesoporous containing activated carbon. The modification via nitrogen doping of activated carbon with NH_4Cl or urea doping led to a decrease in mesopore volume; consequently, the undoped activated carbon exhibited high specific capacitance value in supercapacitors with organic electrolyte. Notably, the nitrogen-doped PS activated carbon, PS-HWZA, demonstrated high rate capability in organic electrolyte due to its retention of mesoporous structure. Optimizing the mesopore content in nitrogen-doped biobased activated carbon plays a crucial role in enhancing capacitance.

Publications and Presentations

1. Vituruch Goodwin, Parinya Jitreewas, Thanathon Sesuk, Pimpa Limthongkul Sumittra Charojrochkul, “Development of Modified Mesoporous Carbon from Palm oil Biomass for Energy Storage Supercapacitor Application”, IOP Conf. Series: Earth and Environmental Science 1199 (2023) 012003.
2. Vituruch Goodwin, Thanathon Sesuk, Parinya Jitreewas, “Biobased Activated Carbon from Palm Biomass Enhancing with Acid Treatment as Supercapacitor electrode Materials”, The 22nd International Symposium on Eco-materials Processing and Design (ISEPD2024) 21 – 24 January 2024, Nakhon Ratchasima, Thailand.
3. Vituruch Goodwin, Thanathon Sesuk, Parinya Jitreewas, “Biobased Activated Carbon from Palm Biomass Enhancing with Acid Treatment as Supercapacitor electrode Materials”, Science and Innovation of Advanced Materials, SIAM journal, (submitted)

1.2 Surface Modifications of Catalysts in Nanoscale for Improvement of Selectivity of Photoconversion of Biomass Related Compounds and Environmental Pollutants

Researchers

1. Prof. Dr. Takashi Sagawa	Graduate School of Energy Science, Kyoto University
2. Assoc. Prof. Dr. Surawut Chuangchote	Department of Tool and Materials Engineering, King Mongkut's University of Technology Thonburi (KMUTT)
3. Dr. Verawat Champreda	National Center for Genetic Engineering and Biotechnology (BIOTEC), NSTDA
4. Prof. Dr. Navadol Laosiripojana	Joint Graduate School of Energy and Environment (JGSEE), King Mongkut's University of Technology Thonburi (KMUTT)

Abstract

Photocatalytic processes for chemical decomposition of biomass related compounds and purifications of wastewater containing environmental polutants are considered as important renewable energy technologies and innovations in terms of efficient utilization of solar energy for materials conversion. This work focused on the materials design of photocatalysts for the photodecomposition of lignin related dimers and purification of wastewater including phenol derivatives. The photocatalysts were prepared by optimized conditions with surface modifications. In terms of the photodecomposition of lignin related dimers, photoconversion of 2-phenoxy-1-phenylethanol (PP-ol) and 2-phenoxyacetophenone (PP-one) as lignin β-O-4 dimer models with TiO_2 was investigated through theoretical calculations and kinetic analyses. It was found that TiO_2 is inactive against PP-ol and PP-one is photodegradable with TiO_2. While in the case of the purification of wastewater, the photocatalysts were modified using the molecular imprinting technique with 4-hydroxybenzoic acid to create the specific binding cavity for phenol derivatives on the surface of TiO_2. In particular, specific removal of phenol from the mixture with ibuprofen using the molecular imprinted TiO_2 was confirmed. The developments of above those photocatalytic systems provide strong platforms for lignin related dimers and photo-purification of environmental pollutants.

Keyword: Photocatalyst; Lignin dimer conversion; Wastewater purification

Introduction

Photocatalytic materials conversion is considered as a favorable method for degradation of lignin and purification of wastewater due to its environmentally

friendly driving force of energy from sunlight and low cost [1]. TiO_2 photocatalyst has received the most research attention because of its affordability, nontoxicity, high photoactivity, and high chemical stability [2]. The challenges for the photocatalytic reaction are the materials design of the photocatalysts, recycling of them after use, and improving the selectivity of them for some specific target compound. In this work, we described the materials design and modifications of photocatalysts for degradation of lignin and purification of wastewater through the improvement of catalyst specificity by optimization of preparation conditions and surface modifications. The obtained photocatalytic system resulted in remarkable enhancement of conversion efficiency in photodegradation of lignin dimers and photo-purification of environmental pollutants.

Research Summary

(1) Photodegradation of dimer models of lignin by TiO_2:

Effective and selective photodegradation of lignin related dimers, photoconversion of 2-phenoxy-1-phenylethanol (PP-ol) and 2-phenoxyacetophenone (PP-one) as lignin β-O-4 dimer models was investigated by using TiO_2 (P-25).

Photodegradation of PP-ol or PP-one by TiO_2 in 1:1 water/ethanol (v/v) w/wo NaOAc under the irradiation of a 500 W Xe lamp at room temperature was performed and the decrease of the absorbance of PP-ol or PP-one was monitored. The time-course changes in the concentration of PP-ol did not obey the pseudo-first-order kinetics. On the contrary, good linearity was confirmed in the case of PP-one. Therefore, it can be concluded that TiO_2 is inactive against PP-ol (eq. 1) and PP-one is photodegradable with TiO_2 (eq. 2). Number of states of PP-ol and PP-one obtained by DFT calculations are indicated in Figure 1. Since LUMO of PP-one is 1 eV below that of PP-ol, PP-one is relatively easy to reduce. Furthermore, charge densities of PP-ol and PP-one are shown in Figure 2. Relatively low densities of αC and O bound to αC of PP-ol against those of PP-one can be seen in Figure 2. Since it was known that radical formation of αC and/or O bound to αC is essentially required for β-O-4 scission [3], PP-one is more reactive than PP-ol in terms of β-O-4 dimer decomposition.

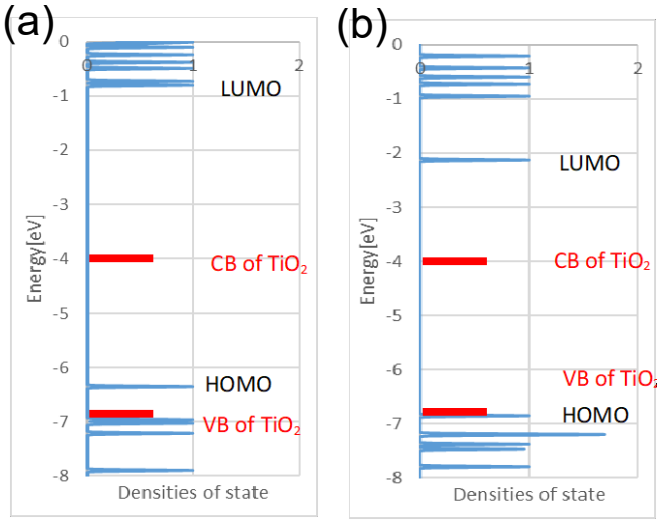

Figure 1. Number of states of PP-ol (a) and PP-one (b) with CB and VB of TiO_2.

From the pseudo first-order plots for photoconversion of PP-one (0.042 - 0.070 mmol dm^{-3}) with NaOAc (0 or 0.035 mmol dm^{-3}), the rate constants were estimated and compared. It was found that there is no remarkable changes in terms of the rate constants in the above reaction conditions. Furthermore, the estimated rate constants were replotted as a Lineweaver Bulk plot. Michaelis-Menten parameters are summarized in Table 1.

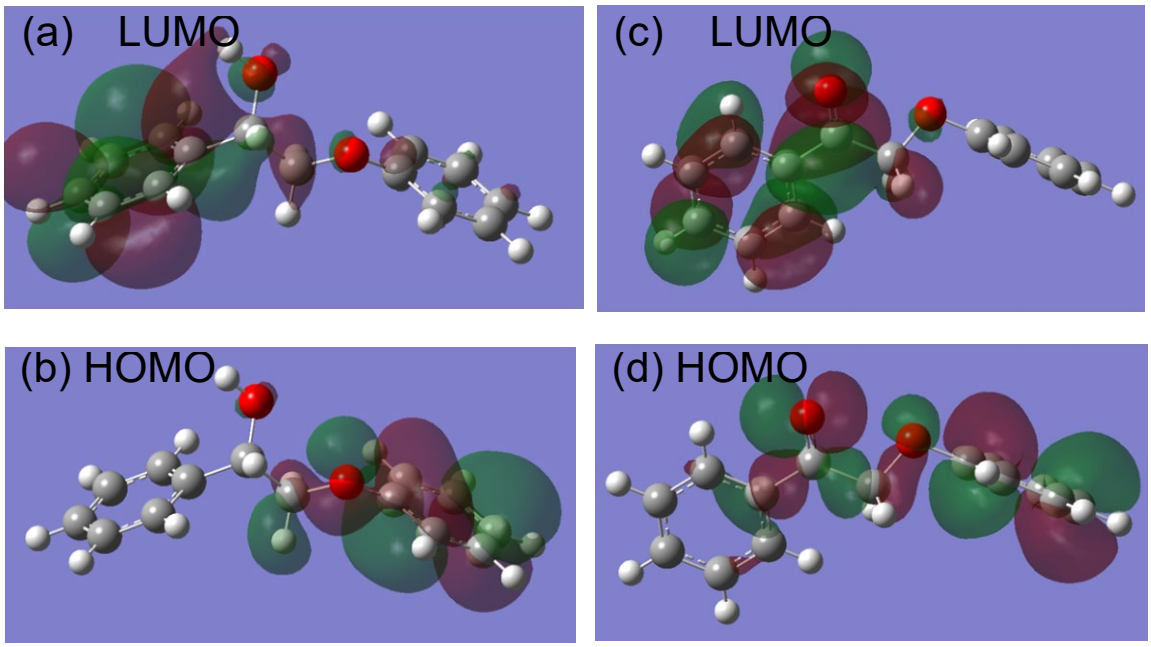

Figure 2. Charge densities of PP-ol (a, b) and PP-one (c, d).

Table 1. Michaelis-Menten parameters for photo-conversion of PP-one (0.042～0.070 mmol dm^{-3}) with NaOAc (0 or 0.035 mmol dm^{-3})

[NaOAc] [mmol dm^{-3}]	K_M [mmol dm^{-3}]	V_{max} [mmol dm^{-3} s^{-1}]	V_{max}/K_M [s^{-1}]
0	0.260	0.00747	0.0288
0.035	0.601	0.0135	0.0224

Michaelis constant (K_M) and apparent maximal rate constant (V_{max}/K_M) after the formation of TiO_2-PP-one complex were estimated. Larger V_{max} was obtained in the presence of NaOAc. On the other hand, higher affinity $1/K_M$ for predominant formation of TiO_2-PP-one complex and larger V_{max}/K_M without NaOAc were attained. Although the net roll of NaOAc in this reaction is still uncertain, it might be possible to regulate and optimize the selectivity of the decomposed product such as the yields of acetophenone, phenol, and so on (eq. 2) by changing the amount of NaOAc and other conditions of this system in future.

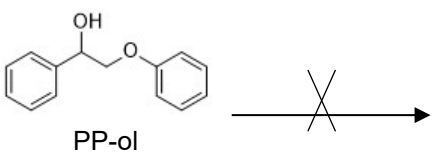

PP-ol

(1)

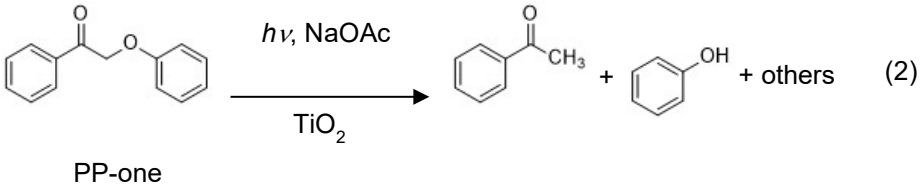

PP-one

(2) Removal of phenol from the mixture of organic pollutants using molecular imprinted TiO_2:

In this part, molecular imprinted technology has been employed to remove phenol from wastewater selectively. The photocatalysts were synthesized using TiO_2 as the platform for template binding using 4-Hydroybenzoic acid. The photocatalysts were annealed at various temperatures, 400°C, 500°C and 600°C. According to the XRD results, it is proved that the samples annealed at 500 °C showed peaks corresponding to [110], [101], [111], [211], and [002] planes [4]. Quantitative analysis of anatase-rutile mixtures was studied by Spurr and Myers as shown in Table 2, where the phase compositions between anatase and rutile in percentage were 75:25, 94.47:5.53, 98.10:1.90, 95.10:4.90, 85.93:14.07, and 62.51:37.49 for P-25, N500, M400, M500, and M 600, respectively. Due to the delayed recombination, Degussa P-25 has a strong photoreactivity.

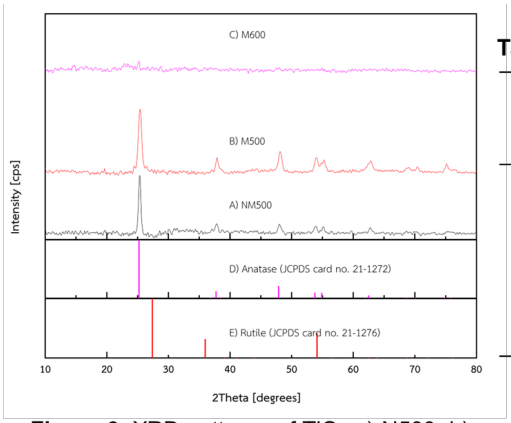

Figure 3. XRD patterns of TiO_2 a) N500, b) M500, c) M600 , d) Anatase and e) rutile

Table 2. Phase composition from Spurr & Myers

Sample Name	Phase Composition Percentage (%)		
	Anatase	Rutile	Brookite
P-25	75.00	25.00	0
N500	94.47	5.53	0
M400	98.10	1.90	0
M500	95.93	4.07	0
M600	62.51	37.49	0

Selective photocatalytic degradation of target pollutant was carried out in a photoreactor equipped with a 75 W Xenon arc lamp placed behind the cuvette cells within 10 cm. In each batch, about 0.1 mg of photocatalysts per 3 mL of pollutants were added to the synthetic wastewater containing selective and non-selective target pollutants. The mixture was stirred vigorously for 150 min. The quantification of phenol remaining in the sample was performed by using high-performance liquid chromatography (HPLC). The results revealed that $MITiO_2$ annealed at 500 °C showed the best photocatalytic degradation of phenol, reaching up to 91.66%, as shown in Figure 4. In contrast, $NMITiO_2$ showed lower removal efficiencies compared to $MITiO_2$, due to the lack of recognition sites on the TiO_2 surface, resulting in lower binding affinity towards

phenol. The photocatalytic tests were further carried out to study their reaction kinetics using the Lineweaver Burk plot. The study showed that samples annealed at 500 °C had lower K_m value and higher V_{max}, suggesting higher estrone binding affinity and catalytic activity. To ensure the safety of releasing the treated wastewater into the environment, TOC analysis was conducted to quantify the total organic carbon remaining in the samples, and it was found that after 360 min of photoreaction, 99.41% of organic carbon has been removed, indicating that a majority of organic compounds including their intermediates have been completely degraded.

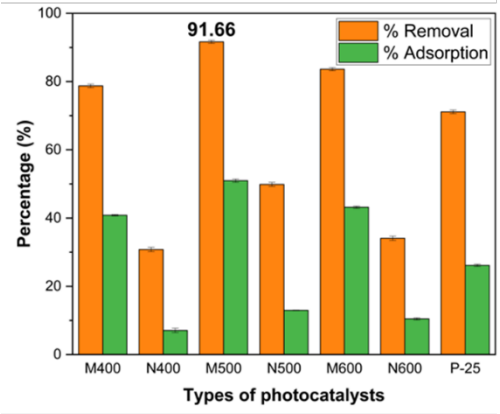

Figure 4. Removal and adsorption efficiency of phenol

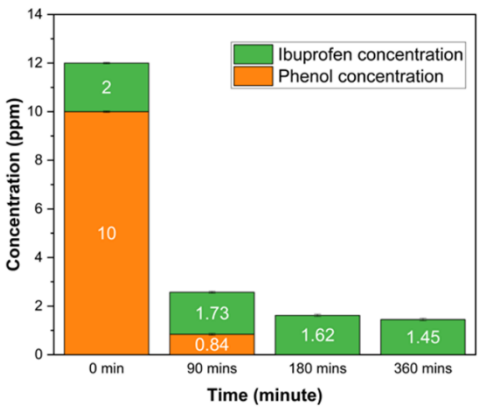

Figure 5. Selective removal efficiency of phenol in mixture of organic pollutants

Figure 5 shows the selective photocatalytic degradation of phenol mixed with ibuprofen as a non-target pollutant. The results proved that even in a mixture of organic pollutants, MITiO$_2$ catalysts still play their roles in selectively removing the pollutants that were imprinted on the platform. 4HBA was chosen as the template due to its shape similarity, and compared to 2-HBA and 3-HBA, which have the hydroxyl group attached to the ortho and meta positions, respectively, 4-HBA exhibits distinct intramolecular and intermolecular characteristics. These differences can result in variations in chemical reactivity, physical properties, and potential applications of the compound [5]. As shown in Figure 6, after template binding and removal, the catalysts selectively bonded with phenol only. Throughout the whole reaction, while UV light is irradiated, the catalysts create two different degradation pathways, including the photoreductive and photooxidative pathways (credited Ms. Phouvnieth Phearum).

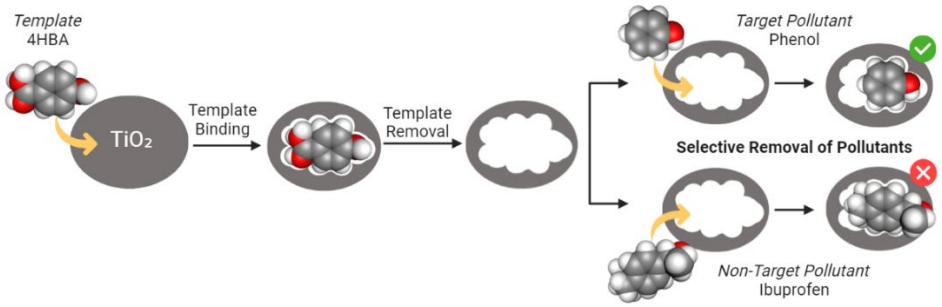

Reference

1. Rafiq, A.; Ikram, M.; Ali, S.; Niaz, F.; Khan, M.; Khan, Q.; Maqbool, M. 2021, *J. Industrial Eng. Chem.*, **2021**, *97*, 111-128.
2. Das, A.; Adak, M.K.; Mahata, N.; Biswas, B. *J. Mol. Liq.*, **2021**, *338*, 116479.
3. Liu, X.; Jiang, Z.; Cao, X.; Shen, Z.; Zhao, W.; Wang, F.; Cui, M.; Liang, C. *ACS Sustainable Chem. Eng*. **2023**, *11*, 14947–14959.
4. Tran.t, T.; Li, J.; Feng, H.; Cai, J.; Yuan, L.; Wang, N.; Cai, Q. *Sens Actuators B Chem* **2014**, 190, 745–751.
5. Albarran, G., Esparza, M., & Mendoza, E. *Radiation Physics and Chemistry*, **2014**, 107, 109–114. https://doi.org/10.1016/j.radphyschem.2014.10.006

Publications and Presentations

Chuangchote, S.; Roongraung, K.; Suriyachai, N.; Champreda, V.; Laosiripojana, Okazaki, Y.; Hachiya, K.; Sagawa, T. "Photocatalytic Degradation of Pollutant and Conversion of Biomass to Value-Added Chemicals," The 8th Japan-ASEAN Science, Technology and Innovation Platform-Work Package 2 on Energy and Environment (JASTIP-WP2) Annual Workshop at Thailand Science Park (TSP), The National Science and Technology Development Agency (NSTDA), Khlong Luang, Pathun Thani, Thailand (Hybrid Workshop), 9 Jan 2024.

Group Workshops, meetings, and researcher exchange

Ms. Rattana Muangmora of KMUTT had stayed at Kyoto University from 13 Mar 2023 to 12 May 2023.

Dr. Surawut Chuangchote and Dr. Patiya Kemacheevakul of KMUTT had dropped in Kyoto University on 28 Mar 2023.

Dr. Takashi Sagawa of Kyoto University, Dr. Surawut Chuangchote of KMUTT, and Dr. Verawat Champreda of NSTDA had discussed the future work on 9 Jan 2024 at Thailand Science Park.

Dr. Takashi Sagawa of Kyoto University visited to KMUTT and discussed the prospect for future collaboration with Dr. Surawut Chuangchote of KMUTT and Dr. Navadol Laosiripojana of JGSEE/KMUTT on 18 Mar 2024.

Other outcomes

N.A

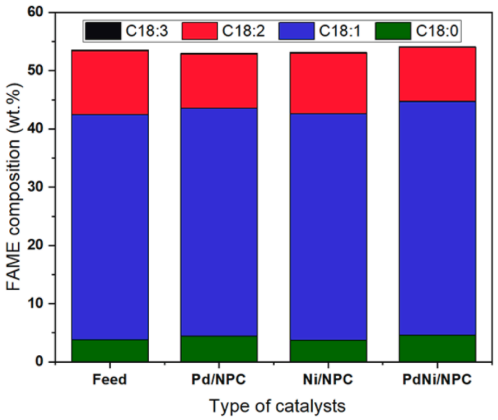

Fig. 10. Effect of monometallic and bimetallic of PdNi on C18 composition (reaction temperature = 100 °C, H_2 pressure = 4 bar and reaction time = 4 h).

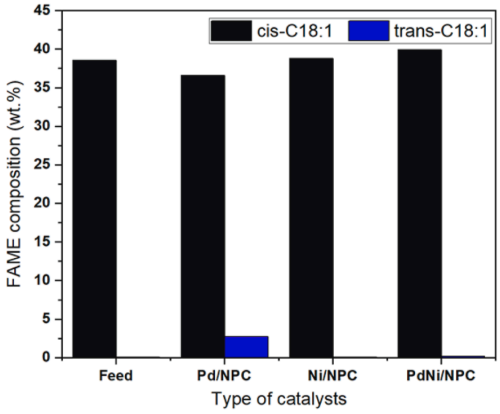

Fig. 11. Effect of catalyst type on cis/*trans*-isomer of C18:1 composition (reaction temperature = 100 °C, H_2 pressure = 4 bar and reaction time = 4 h).

1. Enhancing the Hydrodeoxygenation and Isomerization using Re Nanoparticles Decorated on Ni/SAPO-11 Catalysts for Direct Production of Low-Cold Flow Diesel from Triglycerides

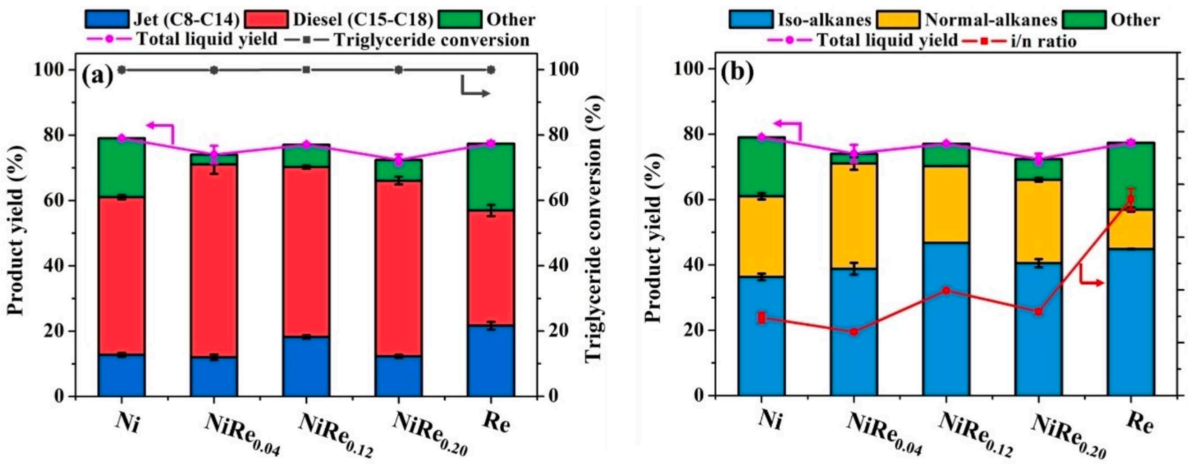

Jet (C8-C14)
Diesel (C15-C18)
Other
Total liquid yield
Triglyceride conversion
(a)
Product yield (%)
Triglyceride conversion (%)
0
20
40
60
80
100
Ni
NiRe0.04
NiRe0.12
NiRe0.20
Re
Iso-alkanes
Normal-alkanes
Other
Total liquid yield
i/n ratio
(b)
Product yield (%)
i/n ratio
0
1
2
3
4
5
6

2.

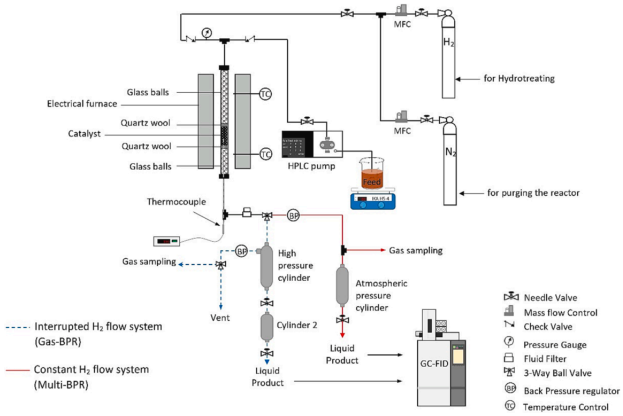

Fig. 1. The trickle bed reactor setup for bio-hydrotreated diesel production.

1.4.2 Fuel Flexibility for Generating Facilities in the Low-Carbon Future: Computational Risk Assessment and Techno-Economic Analysis of Agricultural Wastes Co-Firing in Thermal Power Plants

Publications List:

Rahman, M.N., Yusup, S, Chin, B.L.F., Shariff, I., Quitain, A.T., 2023. Oil Palm Wastes Co-Firing in an Opposed Firing 500 MW Utility Boiler: A Numerical Analysis. CFD Letters 15(3), 139-152. https://doi.org/10.37934/cfdl.15.3.139152

Principal Investigator

Ir. Dr. Mohammad Nurizat Rahman

Energy Markets and Strategy, Energy Systems, DNV Technology Centre, 118227 Singapore

Ir. Dr. Suzana Yusup

Fuels and Combustion, Generation and Environment, TNB Research, 43000 Malaysia

1. Introduction

Presently, the electricity industry is responsible for about 40% of global carbon dioxide (CO_2) emissions, and electricity demand is expected to grow by more than 50% by 2040 [1-2]. Due to the huge reserves and affordability of coal, coal-fired thermal power plants produce a significant share of the world's primary electricity [2-6]. Since coal has a high carbon content, coal-fired thermal power plants generate more CO_2 than any other form of power generation [7-8], and they are one of the main anthropogenic CO_2 emission sources [2, 4, 9], contributing for 30.4% of global CO_2 emissions in 2018 [10]. The reduction of greenhouse gas (GHG) emissions is essential for addressing climate change triggered by global warming, and the reduction of CO_2 emissions is now a global consensus [7, 9-13]. The desire to achieve a low-carbon society is widely discussed, and coal-fired utilities are under increasing pressure to decarbonise [5].

At the United Nations Climate Change Conference (COP26), more than 40 countries pledged to abandon coal [2]. Amidst the excitement surrounding the low-carbon transition, the current global energy crisis has resulted in a renewed rush for coal, showing that the rapid shift to renewable resources may be much more challenging than expected [2]. One remedy for this issue is to progressively phase out coal to allow time for zero-carbon technology to take root [2]. As a result, decreasing carbon emissions from existing coal-fired power plants is essential for lessening the carbon apex and creating a carbon-neutral society while targeting towards zero-carbon technologies and for the supply chain to mature [9-10].

Hence, numerous strategies are being developed to decrease CO_2 emissions from the above said power plants, such as ultra-supercritical technology [10], integrated gasification combined cycle (IGCC) [10], double reheat technology [10], carbon capture and storage (CCS) [10], oxy-fuel combustion [7], carbon capture and storage [7], and the use of low-

carbon/carbon-neutral fuels [10-11]. When it comes to the use of low-carbon/carbon-neutral fuels, hydrogen is anticipated to play a significant part in the future formation of a low-carbon society [9, 11-13, 15]. Nevertheless, due to its high volatility [11], hydrogen storage and transportation remain complicated [13, 16]. Biomass and biogas are also alluring carbon-neutral fuels for co-firing [5, 14], but seasonal fluctuations in feedstock supply pose major challenges [5].

Malaysia has an advantage in this regard due to the abundance of palm oil plantations [17], where oil palm wastes (OPWs) are one of the readily accessible biomass resources [6, 18]. Solid waste from palm oil plantations, such as empty fruit bunches (EFB), palm kernel shell (PKS), and palm mesocarp fibres (PMF), has the potential to be used as a fuel to generate electricity [6, 18]. The use of OPWs in a coal-fired power plant can significantly reduce GHG emissions [6]. Furthermore, using OPWs as fuel in coal-fired power plants could mitigate one of the negative effects of palm oil plantations, which is the massive production of agricultural waste [6, 19]. Plus, the majority of newly built coal-fired power plants in some European countries, Japan, and China are largely co-fired, with biomass accounting for 10%-20% of calorie output [6]. Therefore, with efficient planning of the OPWs supply chain to achieve the co-firing scales required [6], there will be a significant business opportunity for OPWs co-firing.

However, a few co-firing repercussions must be identified and clearly understood in terms of OPWs co-firing suitability in existing coal-fired power plants. Nowadays, to remain economically viable, coal-fired power plants must overcome the challenge of non-design, low-quality coal usage, which incurs major operational issues such as greater water wall slagging and high temperature corrosion [20]. Therefore, OPWs co-firing may result in unexpected and undesirable problems with boiler operation, efficiency, corrosion, erosion, flame stability, slagging, fouling, heat adsorption in the furnace, and so on [21].

In coal-fired power plants, the co-firing technique involves injecting different types of solid fuels into the boiler from a different burner with no prior mixing. Since it is challenging to transport and disseminate two solid fuels separately to bunkers, this method is not widely employed in power plants [21]. Nonetheless, co-firing has shown greater ability to manage co-firing adjustment between two or more different types of solid fuels [22]. However, the majority of solid fuels blending research has focused on the combustion characteristics of the out-furnace blending strategy, in which various types of solid fuels were pre-mixed before entering the boiler [23]. Hence, there is a need to evaluate co-firing strategy since most research has focused on the combustion aspects of the out-furnace blending procedure, and the underlying combustion mechanisms resulting from the OPWs co-firing strategy are still vaguely defined and limited to academic studies [6, 24].

Coal is a heterogeneous substance with varying qualities such as rank, maceral content, and impurities [23]. As a result, constructing an ideal methodology for predicting the combustion behaviour of coals and OPWs co-firing is challenging [23]. It has been established that fuel composition characteristics (proximate and ultimate analysis data, heating value, etc.) remain additive after blending, whereas many combustion characteristics are non-additive [23-24]. That is, they have both reactive and unreactive consequences [23-24]. Additivity, for example, cannot predict ignition, flame stability, slagging, fouling, and nitrogen

oxides (NO_x) emissions [23-24]. Experimental techniques were used to assess the combustion performance of various types of solid fuel blends used in pulverised coal-fired boilers [24]. Several empirical indices based on volatile matter constituents, fuel ratios, and maceral compositions were also built from the experimental results in order to empirically predict the slagging, fouling, ignitability, flame stability, and burning of coal-OPWs [25].

Another approach that has the potential to be a dependable and cost-effective strategy in the investigation of OPWs co-firing is numerical modelling (computational fluid dynamics). Numerical modelling has been shown to be an effective technique for diagnosing and resolving flow and combustion issues [24, 26-31]. As it can provide insights into the combustion properties of unfamiliar solid fuel blends [6, 24], such as OPWs co-firing, it has been widely used to examine the combustion performance of a single coal and multiple solid fuel blends in bench-pilots and full-scale utility furnaces. Lee *et al.* [24] simulated combustion and flow for a variety of solid fuel blends, and the numerical modelling was validated using experimental data from a drop-tube furnace. They revealed that the combinatorial impact is caused by particle temperature and volatile matter interactions between individual solid fuels, and the modelling offers an effective strategy for the implementation of multiple solid fuel blends.

Aziz *et al.* [6] implemented the OPWs co-firing with coal in a utility coal-fired boiler model, using PKS as the OPW type. While the assessment has provided significant findings on the predicted co-firing behaviour in the aspects of emissions and thermal behaviour, the validation aspect of the said assessment is vague with no actual power plant operational data involved. In broad sense, the combustion characteristics, heating surface temperatures, and flue gas components from pilot-scale tests differ from actual power plant data [32-33], and the said operating data differs even between power plants. Pilot-scale test data is frequently obtained from shorter test durations, which differs from the real operating procedure in power plants, in continuous mode of operation and longer combustion period. As a result, creating numerical models based on data from pilot-scale experiments will not provide a comprehensive insight of actual OPWs co-firing in a utility boiler.

To create a credible OPWs co-firing numerical model, extensive data collection activities at the actual coal-fired utility boiler, as well as numerical procedures that closely follow the actual coal-fired utility boiler operations, are highly desired. Another reason for using actual data is the complicated geometry of coal-fired utility boilers, which affects the solid phase flow behaviour and alters particle movement and fluid dynamics within the boiler [34]. Particle and flow dynamics have a large impact on the subsequent thermal behaviour [34].

To address the stated gaps, the present study collects relevant power plant data from one of Malaysia's 500 MW opposed-fired coal-fired power plants, allowing the actual plant data to be appropriately defined and transformed into a reliable OPWs co-firing numerical model. The validation was carried out using a single coal case as a baseline. The numerical model used in this research was integrated with the solid fuel combustion model, which included the kinetics of devolatilisation, char conversion/reaction, and volatiles reactions. The current study employed three types of OPWs including EFB, PKS, and PMF. The primary objective of

the current research is to gain fundamental insights into the operational impacts of various types of OPWs co-firing in a utility boiler.

2. Physical Setup

The three-dimensional (3D) configuration of a coal-fired boiler as shown in Figure 1 was created using as-built dimensions from the actual coal-fired power plant under consideration. The boiler has a wall-firing design with 36 coal burners that are also the primary air (PA) inlets, with 36 secondary air (SA) inlets circumferentially positioned at each burner-PA inlet to enable better mixing of the incoming coal and air, as well as to provide a dry low NO_x region closer to the burner area where the incoming SA creates a recirculation zone for the incoming coal and air [35-36]. Each side of a boiler (front and rear walls) has each 18 burner-PA inlets and 18 SA inlets located at three different heights at a burner zone due to the wall-firing layout. To reduce computational costs, the tube bundles of superheaters and reheaters were simplified to a few thin walls [35-36]. The accuracy of computational works considered, heat transfer models' implementation to thin walls to replicate the heat transport process between the flue gas and the steam within the heat exchanger bundles. The heat transfer modelling on the heat exchanger bundles is done in the same way as Yang *et al.* [37].

The over-fire air (OFA) inlets are positioned between the burner zone and the heat exchanger bundles, and they are made up of six inlets at the front and rear walls with the same elevation height. The computational model and boundary names used on the boiler are depicted in Figure 1. Mills 1-6, as shown in Figure 1, supply coal and PA for each burner-PA inlet elevation (A to F).

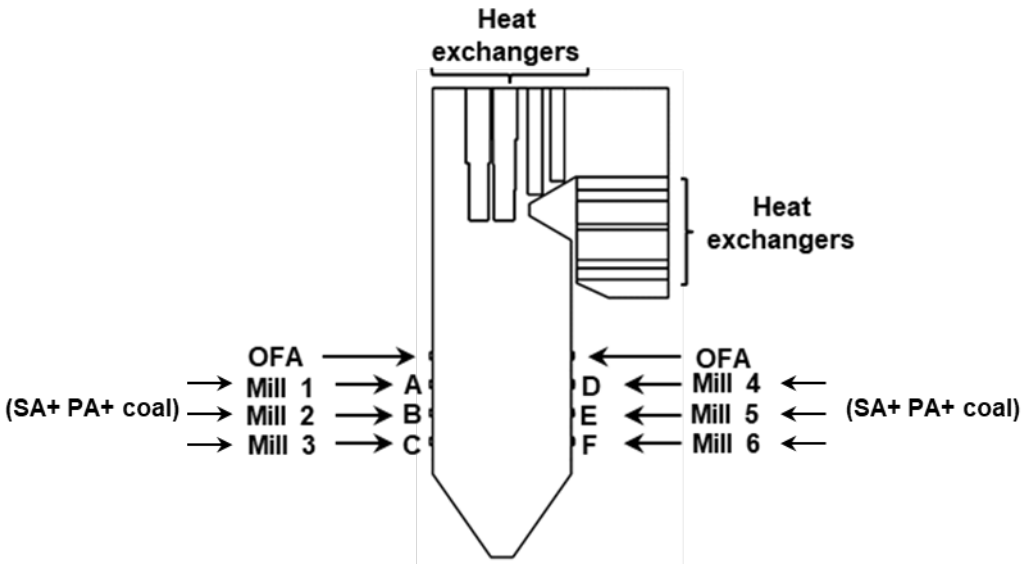

Fig. 1. Computational model of the boiler

In a common utility coal-fired boiler framework, the coal-fired boiler integrates the piping structure and the furnace as one system, with all mills connected to discharge pipes that deliver coal particles and PA into the boiler [35-36]. However, in order to save computational costs, the piping structure is not part of the computational domain for this study. Fuel oil (FO) inlets are not considered as one of the flow inlet boundaries in this study because the FO is frequently used during the furnace's startup phase. The current study is a steadily simulated reacting flow assessment in which combustion is assumed to be long past the transitory period of the coal-fired furnace's start-up operation.

3. Numerical Setup

The detailed chemical reaction modelling schemes of solid fuel combustion used in this research work are similar to those demonstrated in our previous research [35-36]. The chemical kinetics and combustion models used in this study account for the three main stages of solid fuel combustion: devolatilisation, char conversion/reaction, and volatiles reactions. The volatile composition and rate constants for solid fuel devolatilisation were predicted using the advanced solid fuel network model and ascertained using the historical solid fuel database from our own analytical laboratory. The governing equations were discretised using the finite volume technique (steady state and compressible). ANSYS Fluent V.19 R1 was employed for all setup and numerical processing. A pressure-based solver was used to solve the governing equations. To resolve the pressure-velocity coupling, the Semi-Implicit Method for Pressure Linked Equations (SIMPLE) technique was used. Ferziger *et al.* [38] go into great detail about the SIMPLE algorithm's constants and formulations. To address the radiative heat transfer from the reacting flow, the Discrete Ordinates (DO) model was used. To resolve turbulent flow, the Shear Stress Transport (SST) k - w model was utilised, which has been shown to provide good convergence and accuracy in reacting flow simulations [39].

Sieve analysis was performed on coal samples taken from the actual power plant under study to determine the size fraction of coal particles. The size fraction was used to translate the range of coal fineness into the Rosin Rammler distribution, and the Rosin Rammler distribution curve fit coefficients were introduced into the numerical code to reflect the variation of coal fineness from the power plant under study. The fineness of the coal ranged between 75µm and 300µm, and all solid fuel particles were tracked with a Lagrangian system that accounted for turbulent dispersion for 80,000 particles. It is a well-known fact that the pulverised biomass will have larger particle sizes after passing through the conventional coal-fired utility pulverised mill due to the difference in density, Hardgrove Grindability Index (HGI), and terminal velocity [40]. The fineness of OPWs is therefore assumed to be in the range of 75µm for this research, as required by the power plant. The impact of HGI is excluded in this co-firing research and will be investigated further in the future.

A post-processing method was used to simulate NO_x production. To begin, combustion simulations were used to derive temperature, major gas composition, and velocity distributions. The reactions of thermal NO_x and NO_x reduction by char were then incorporated

based on the combustion computation. Only NO_x-related species were computed, but flow, turbulence, other major gas compositions such as oxygen, CO_2, carbon monoxide (CO), and hydrogen, energy, as well as radiation equations were not solved.

The bituminous coal was chosen for this study because the current boiler was designed to only burn bituminous coal. Table 1 displays the properties of the solid fuels (coal and OPWs) used in the simulations. The said bituminous coal was used by the power plant while it was operating, and it was collected in a small sample and subjected to extensive analytical fuel testing to determine its coal properties. The properties of OPWs were provided by one of Malaysia's major OPW suppliers. These solid fuel characteristics (shown in Table 1) are part of the numerical study's boundary conditions. Table 2 depicts the four (4) solid fuel co-firing scenarios used in the simulation. The OPWs co-firing ratios were determined based on a calorific percentage (cal. %).

Table 1

Solid fuel types and characteristics

Solid fuel	Proximate analysis, wt. %, dry basis (db) (VM-Volatile matter, FC-Fixed carbon, AC-Ash content)			Ultimate analysis, wt. %, db (C-Carbon, H-Hydrogen, N-Nitrogen, O-Oxygen, S-Sulphur)					GCV- Gross Calorific Value, db (kcal/kg)
	VM	FC	AC	C	H	N	O	S	
Coal (B1)	25.4	59.5	15.1	73.68	4.53	1.65	4.57	0.50	6678
EFB	78.5	17.3	4.3	44.07	5.52	0.41	45.73	0.46	5067
PKS	80.9	16.8	2.4	49.13	5.42	0.48	42.45	0.41	4852
PMF	79.8	14.9	5.4	45.51	5.03	0.54	43.61	0.42	4876

Table 2

Co-firing cases

Case	Fuel type for the burner row						Capacity (MW)
	A (20 cal.%)	B (20.cal%)	C (20.cal%)	D (20.cal%)	E (20.cal%)	F (20.cal%)	
Baseline	B1	B1	B1	Standby	B1	B1	500
B1-EFB	EFB	B1	B1		B1	B1	
B1-PKS	PKS	B1	B1		B1	B1	
B1-PMF	PMF	B1	B1		B1	B1	

According to Tables 1 and 2, coal B1 is bituminous, whereas EFB, PKS, and PMF are OPWs. The baseline scenario involves no co-firing (100% coal B1). The validation with actual plant data was carried out based on the CFD results from the aforementioned baseline case. This is because the baseline case, or 100% coal B1, has been used frequently in the power plant under study, and a large amount of plant data from this firing can be utilised to validate the baseline case. Therefore, the power plant operating condition during the firing of coal B1 was

properly captured by the power plant sensor and transferred as the boundary conditions of the current numerical analysis. Mills 1-6 deliver coal and PA for each burner-PA inlet elevation, as shown in Table 3. Mill 4 emits no coal flow at the burner elevation D because it was used as a standby burner.

Table 3

Operating conditions for the CFD model validation

Parameter	Operating condition
Mill 1 coal flow (t/h)	32.91
Mill 2 coal flow (t/h)	38.45
Mill 3 coal flow (t/h)	39.45
Mill 4 coal flow (t/h)	0.00
Mill 5 coal flow (t/h)	39.45
Mill 6 coal flow (t/h)	39.45
Main steam temperature (°C)	538
Total OFA flow (t/h)	389.36
Total SA flow (t/h)	1168.07
Mill 1 PA inlet temperature (°C)	78.99
Mill 2 PA inlet temperature (°C)	79.95
Mill 3 PA inlet temperature (°C)	79.83
Mill 4 PA inlet temperature (°C)	79.95
Mill 5 PA inlet temperature (°C)	79.95
Mill 6 PA inlet temperature (°C)	48.89
Mill 1 PA flow (t/h)	73.86
Mill 2 PA flow (t/h)	72.90
Mill 3 PA flow (t/h)	73.85
Mill 4 PA flow (t/h)	73.78
Mill 5 PA flow (t/h)	68.26
Mill 6 PA flow (t/h)	14.92
SA temperature (°C)	333.00

4. Grid-Convergence Analysis and Model Validation

To assure that the spatial convergence accuracy is sufficient, the grid independent test is performed. Meshes (elements) are built with orthogonal quality and skewness in mind to reflect mesh attributes that influence the level of spatial discretisation errors [35-36]. To ensure that acceptable mesh qualities could be constructed, the orthogonal and skewness features of all generated meshes in the grid independent test were controlled. When the mesh number exceeds 1.89 million, the velocity and temperature profiles in the furnace's centre nearly stop changing. Figure 2 depicts the mesh model.

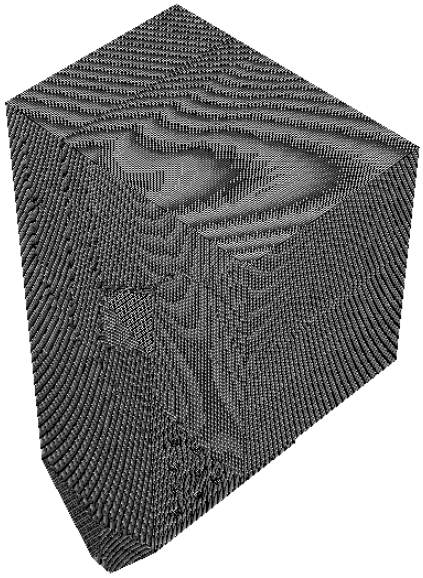

Fig. 2. Mesh model of the boiler (isometric view)

After determining the independent mesh number, a model validation exercise was performed, which involved comparing the predicted furnace exit gas temperature (FEGT) result from the current model to the actual FEGT from the power plant under study. The predicted FEGT value is based on the average temperature in a plane slightly below the nose area of the furnace (below the tube bundles of superheaters and reheaters). The FEGT results from the CFD model and the actual power plant are shown in Table 4. Table 4 shows that the overall CFD model predicted results were within 10% of the actual FEGT. As a result, the current numerical model's reliability was determined to be acceptable based on the FEGT validation results.

Table 4

Validation based on FEGT results

FEGT (°C)		Percentage difference (%)
Actual	CFD	
1200	1284.81	7.07

5. Results and Discussion

5.1. Temperature Results

Figure 3 depicts the predicted temperature contour of the boiler model as well as the nose area temperature for each case. Since OPWs have a higher VM than baseline coal, the high combustion temperature zones in the boiler with OPWs co-firing are much larger than in the boiler with pure coal firing. Previous research has shown that the VM plays an important role in the early combustion phenomenon and the oxidation of large amounts of volatiles [17, 36].

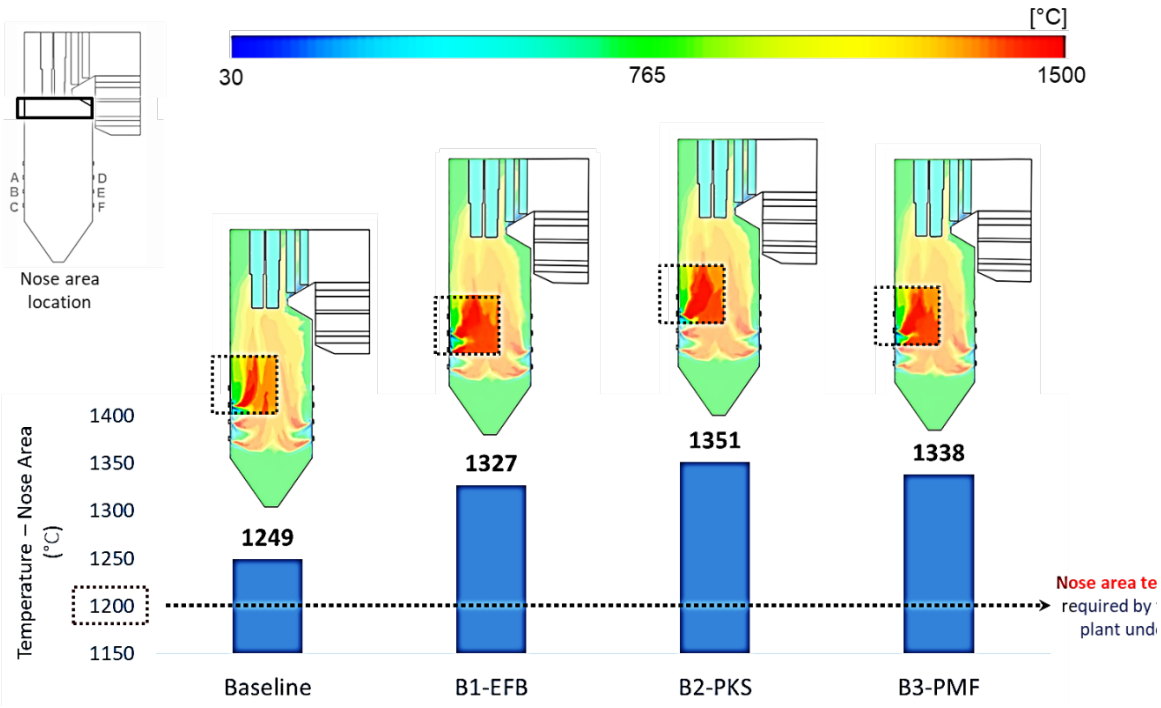

Fig. 3. Predicted temperature results within the boiler model

The predicted nose area temperature, which exceeded 1200°C in all OPWs co-firing cases, is the highlight of these findings. The power plant under consideration requires an approximately 1200°C at the nose area region to avoid ash deposition occurrences, with the nose area temperature not exceeding the initial deformation temperature (IDT) of the solid fuel blends. As previously stated, the power plant under study was intended to burn primarily bituminous coals, a low VM solid fuel [36]. As a result, the boiler configuration and operating conditions were primarily designed to ensure that bituminous coals could be fired while maintaining a nose area of roughly 1200°C.

Co-firing OPWs fuel, which has a high VM, could change the kinetics time scale of devolatilisation, which is already known to be shorter than the time scale of successive char combustion [36]. The synergistic impact of coal and OPW kinetics aids in raising the combustion rate of solid fuel blends,B1 coal, which has prospered from OPW's higher combustibility, proceeds to have a greater rate of volatile release and char combustion.

5.2. Unburned Carbon (UBC) Results

Excessive UBC in fly ash is undesirable from the standpoint of power plant operation. It represents a noticeable fuel loss, lowering overall plant efficiency [41]. The concrete industry is the largest market for fly ash (additive for cement) [41]. According to ASTM standard 618, one of the criteria for such an application is that the UBC or loss on ignition (LOI) limit must be less than 6% [41]. Therefore, power plant places a lot of importance on UBC amount because it affects their profits. UBC levels above the LOI limit reduced plant efficiency, and fly ash could not be sold to the concrete industry. As seen in Table 5, the predicted UBC levels at the boiler's outlet are reduced when co-firing with OPWs because the OPWs-coal blends contain less FC than the pure coal blend.

Table 5

Predicted UBC levels

Case	CFD (%)	LOI limit (%)
Baseline	3.52	<6
B1-EFB	2.03	
B1-PKS	1.97	
B1-PMF	1.94	

5.3. OPWs Fuel Flow and Mill Capacity

In order to achieve the required load from the boiler, the fuel flow into the boiler was primarily determined by its calorific output. The required load for this utility boiler is 500 MW.

As shown in Figure 1, the pulverised solid fuel will be transported from the mill to the boiler. Table 2 shows that in all OPWs co-firing cases, 20 cal.% of the OPWs will be injected into the boiler, accounting for the usage of one mill (in this case Mill 1/burner row A). Figure 4 depicts the calculated OPWs fuel flow for each OPWs co-firing case.

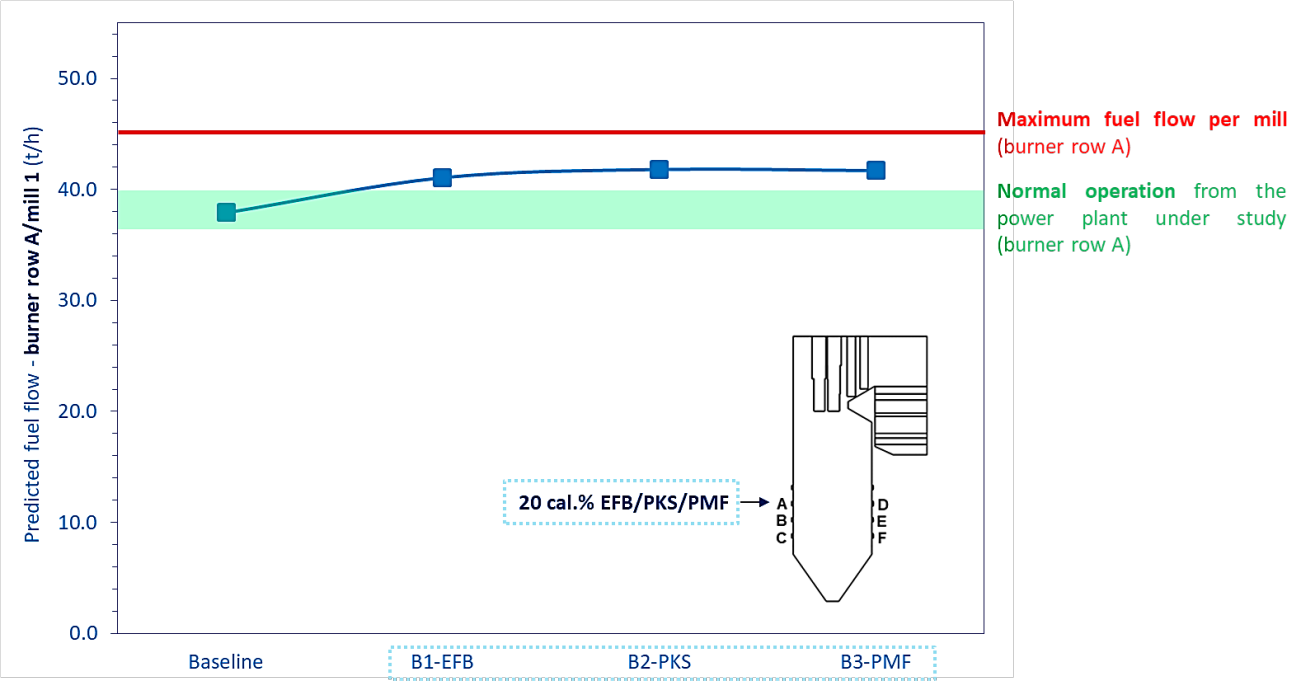

Fig. 4. Calculated OPWs fuel flow per mill (burner row A)

Figure 4 shows that the OPWs fuel flow is slightly higher than the normal operation of the power plant under consideration. This is due to OPWs having a lower GCV than B1 coal, as shown in Table 1. As seen in the baseline case (pure coal firing), the fuel flow at burner row A is within normal operation due to the use of B1 coal at burner row A. The slight increase in OPWs fuel flow corresponds to lower GCV of OPWs when compared to B1 coal. As a result, a higher OPWs fuel flow is required to achieve the utility boiler's required load. Nonetheless, as shown by the red line in Figure 4, the predicted OPWs fuel flow is still lower than the maximum allowable fuel flow per mill.

5.4. Predicted CO, CO_2, and NO_x

Tables 6, 7, and 9 show the predicted CO_2, CO, and NO_x at the boiler's outlet, respectively. OPWs have lower FC than coal, resulting in lower CO and CO_2 emissions when coal is co-fired

with OPWs. However, because ash mineral compositions are not taken into account, even though OPWs contain less N than the baseline coal, OPWs co-firing cases are expected to produce more NO_x than the baseline coal due to the higher flame temperature generated, which results in an increase in thermal NO_x, as stated in the Zeldovich mechanism [6]. Except for the predicted NO_x, the predicted CO emissions do not exceed the specified emission limit required by the power plant under study.

Table 6

Predicted CO levels

Case	CFD (mg/m^3)	Limit (mg/m^3)
Baseline	197.35	<200
B1-EFB	149.41	
B1-PKS	147.86	
B1-PMF	147.11	

Table 7

Predicted CO_2 levels

Case	CFD (%)	Limit (%)
Baseline	14.05	N/A
B1-EFB	9.53	
B1-PKS	8.82	
B1-PMF	8.45	

Table 8

Predicted NO_x levels

Case	CFD (mg/m^3)	Limit (mg/m^3)
Baseline	574	<600
B1-EFB	671	
B1-PKS	695	
B1-PMF	673	

6. Conclusions and Recommendations

The assessment of OPWs co-firing for one of Malaysia's 500 MW utility boilers was numerically carried out. Three types of OPWs tested including EFB, PKS, and PMF. The predicted FEGT from the numerical model was validated against the actual FEGT from the coal-fired power plant where the current boiler is located, revealing a discrepancy of less than 10%. As a result of the validation, the numerical model has the capability to be a reliable and

cost-effective tool for analysing the combustion performance of multiple solid fuel blends in an actual power plant boiler. The current study yielded the following key findings based on numerically tested OPWs co-firing cases:

- The nose area temperature was anticipated to exceed the cap of 1200°C in OPWs co-firing cases due to the higher VM in OPWs than the baseline pure coal case, resulting in a higher rate of volatile release. It is suggested to co-fire OPWs in a boiler designed to burn sub-bituminous coal rather than the bituminous-fuelled boiler used in this study because the VM and FC of OPWs are more comparable with common sub-bituminous coals.
- When co-firing with OPWs, the predicted UBC levels at the boiler's outlet are lower because OPWs-coal blends contain less FC than pure coal blends. Furthermore, UBC levels are expected to be lower than the LOI limit in all cases, demonstrating its positive impact in terms of carbon reduction.
- Slightly reduced mill performance was discovered as a result of the calculated OPWs fuel flow exceeding the normal operation in the power plant under study to compensate for the low GCV of OPWs while achieving the required load from the boiler. As a result of the potential increase in fuel consumption caused by OPW's low calorific value, the cost of operating the power plant that used OPWs co-firing may be higher.
- OPWs co-firing is expected to emit less CO and CO_2 than baseline coal due to lower FC. Nonetheless, higher thermal NO_x was predicted due to the higher flame temperature generated by OPWs co-firing. However, it is recommended that the ash mineral compositions to be included in future numerical studies because the ash minerals may influence the emitted NO_x.

References

[1] Cesaro, Zac, Matthew Ives, Richard Nayak-Luke, Mike Mason, and René Bañares-Alcántara. "Ammonia to power: Forecasting the levelized cost of electricity from green ammonia in large-scale power plants." *Applied Energy* 282 (2021): 116009. https://doi.org/10.1016/j.apenergy.2020.116009

[2] Cardoso, João Sousa, Valter Silva, José Antonio Mayoral Chavando, Daniela Eusébio, and Matthew J. Hall. "Numerical modelling of the coal phase-out through ammonia and biomass co-firing in a pilot-scale fluidized bed reactor." *Fuel Communications* 10 (2022): 100055. https://doi.org/10.1016/j.jfueco.2022.100055

[3] Zhang, Juwei, Takamasa Ito, Hiroki Ishii, Sakiko Ishihara, and Toshiro Fujimori. "Numerical investigation on ammonia co-firing in a pulverized coal combustion facility: Effect of ammonia co-firing ratio." *Fuel* 267 (2020): 117166. https://doi.org/10.1016/j.fuel.2020.117166

[4] Tsukada, Naruhito, Naoki Kinoshita, Yutaka Kabuki, Yuzo Taguchi, Yohei Takashima, Toshikazu Tsumura, and Masayuki Taniguchi. "Role of OH radical in fuel-NOx formation during cocombustion of ammonia with hydrogen, methane, coal, and biomass." *Energy & Fuels* 34, no. 4 (2020): 4777-4787. https://dx.doi.org/10.1021/acs.energyfuels.0c00356

[5] Weng, Wubin, Zhongshan Li, Paul Marshall, and Peter Glarborg. "Participation of alkali and sulfur in ammonia combustion chemistry: Investigation for ammonia/solid fuel co-firing applications." *Combustion and Flame* 244 (2022): 112236. https://doi.org/10.1016/j.combustflame.2022.112236

[6] Aziz, Muhammad, Dwika Budianto, and Takuya Oda. "Computational fluid dynamic analysis of co-firing of palm kernel shell and coal." *Energies* 9, no. 3 (2016): 137. https://doi.org/10.3390/en9030137

[7] Ishihara, Sakiko, Juwei Zhang, and Takamasa Ito. "Numerical calculation with detailed chemistry on ammonia co-firing in a coal-fired boiler: Effect of ammonia co-firing ratio on NO emissions." *Fuel* 274 (2020): 117742. https://doi.org/10.1016/j.fuel.2020.117742

[8] Zhu, Jingji, Xiaowei Liu, Yishu Xu, Jingying Xu, Huakun Wang, Kai Zhang, Xiaobei Cheng, and Dunxi Yu. "Probing into Volatile Combustion Flame and Particulate Formation Behavior During the Coal and Ammonia Co-firing Process." *Energy & Fuels* 36, no. 16 (2022): 9347-9356. https://doi.org/10.1021/acs.energyfuels.2c01450

[9] Wang, Xin, Weidong Fan, Jun Chen, Guanyu Feng, and Xiang Zhang. "Experimental study and kinetic analysis of the impact of ammonia co-firing ratio on products formation characteristics in ammonia/coal co-firing process." *Fuel* 329 (2022): 125496. https://doi.org/10.1016/j.fuel.2022.125496

[10] Xu, Yishu, Huakun Wang, Xiaowei Liu, Jingji Zhu, Jingying Xu, and Minghou Xu. "Mitigating CO_2 emission in pulverized coal-fired power plant via co-firing ammonia: A simulation study of flue gas streams and exergy efficiency." *Energy Conversion and Management* 256 (2022): 115328. https://doi.org/10.1016/j.enconman.2022.115328

[11] Chen, Ping, Yao Fang, Peipei Wang, Mingyan Gu, Kun Luo, and Jianren Fan. "The effect of ammonia co-firing on NO heterogeneous reduction in the high-temperature reduction zone of coal air-staging combustion: Experimental and quantum chemistry study." *Combustion and Flame* 237 (2022): 111857. https://doi.org/10.1016/j.combustflame.2021.111857

[12] Ishihara, Sakiko, Juwei Zhang, and Takamasa Ito. "Numerical calculation with detailed chemistry of effect of ammonia co-firing on NO emissions in a coal-fired boiler." *Fuel* 266 (2020): 116924. https://doi.org/10.1016/j.fuel.2019.116924

[13] Rahman, Mohammad Nurizat, and Mazlan Abdul Wahid. "Renewable-based zero-carbon fuels for the use of power generation: A case study in Malaysia supported by updated developments worldwide." *Energy Reports* 7 (2021): 1986-2020. https://doi.org/10.1016/j.egyr.2021.04.005

[14] Rahman, Mohammad Nurizat, Mohd Haffis Ujir, Mazlan Abdul Wahid, and Mohd Fairus Mohd Yasin. "A single-step chemistry mechanism for biogas supersonic combustion velocity with nitrogen dilution." *Journal of Thermal Analysis and Calorimetry* (2022): 1-15. https://doi.org/10.1007/s10973-022-11356-x

[15] Rahman, Mohammad Nurizat, Norshakina Shahril, and Suzana Yusup. "Hydrogen-Enriched Natural Gas Swirling Flame Characteristics: A Numerical Analysis." *CFD Letters* 14, no. 7 (2022): 100-112. https://doi.org/10.37934/cfdl.14.7.100112

[16] Chen, Ping, Huichun Wang, Boyu Jiang, Ying Wang, Mingyan Gu, Guang Chen, and Xiangyong Huang. "An experimental and theoretical study of NO heterogeneous reduction in the reduction zone of ammonia co-firing in a coal-fired boiler: Influence of CO." *Fuel Processing Technology* 231 (2022): 107184. https://doi.org/10.1016/j.fuproc.2022.107184

[17] Yacob, Noraishah Shafiqah, and Hassan Mohamed. "Investigation of Palm Oil Wastes Characteristics for Co-Firing with Coal." *Journal of Advanced Research in Applied Sciences and Engineering Technology* 23, no. 1 (2021): 34-42. https://doi.org/10.37934/araset.23.1.3442

[18] Wu, Qibai, Thien Ching Qiang, Guoxun Zeng, Haiyan Zhang, Ye Huang, and Yaodong Wang. "Sustainable and renewable energy from biomass wastes in palm oil industry: A case study in Malaysia." *International Journal of Hydrogen Energy* 42, no. 37 (2017): 23871-23877. https://doi.org/10.1016/j.ijhydene.2017.03.147

[19] Subramaniam, Vijaya, Soh Kheang Loh, and Astimar Abdul Aziz. "GHG analysis of the production of crude palm oil considering the conversion of agricultural wastes to by-products." *Sustainable Production and Consumption* 28 (2021): 1552-1564. https://doi.org/10.1016/j.spc.2021.09.004

[20] Purnomo, Fajar, and Atok Setiyawan. "Numerical study on in-furnace blending coal combustion characteristics in a 625 MW tangentially fired pulverized coal boiler." In *AIP Conference Proceedings*, vol. 2187, no. 1, p. 020038. AIP Publishing LLC, 2019. https://doi.org/10.1063/1.5138293

[21] Baek, Se Hyun, Ho Young Park, and Sung Ho Ko. "The effect of the coal blending method in a coal fired boiler on carbon in ash and NO_x emission." *Fuel* 128 (2014): 62-70. http://dx.doi.org/10.1016/j.fuel.2014.02.043

[22] Wang, Chang'an, Qinqin Feng, Qiang Lv, Lin Zhao, Yongbo Du, Pengqian Wang, Jingwen Zhang, and Defu Che. "Numerical investigation on co-firing characteristics of semi-coke and lean coal in a 600 MW supercritical wall-fired boiler." *Applied Sciences* 9, no. 5 (2019): 889. https://doi.org/10.3390/app9050889

[23] Lee, Byoung-Hwa, Eric G. Eddings, and Chung-Hwan Jeon. "Effect of coal blending methods with different excess oxygen on unburned carbon and NO_x emissions in an entrained flow reactor." *Energy & fuels* 26, no. 11 (2012): 6803-6814. https://doi.org/10.1021/ef300562t

[24] Lee, Byoung-hwa, Seoung-gon Kim, Ju-hun Song, Young-june Chang, and Chung-hwan Jeon. "Influence of coal blending methods on unburned carbon and NO emissions in a drop-tube furnace." *Energy & fuels* 25, no. 11 (2011): 5055-5062. https://doi.org/10.1021/ef200783q

[25] Hariana, Feri Karuana, Prabowo, Edi Hilmawan, Arif Darmawan, and Muhammad Aziz. "Effects of Different Coals for Co-Combustion with Palm Oil Waste on Slagging and Fouling Aspects." *Combustion Science and Technology* (2022): 1-23. https://doi.org/10.1080/00102202.2022.2152684

[26] Rahman, Mohammad Nurizat, Mohd Fairus Mohd Yasin, and Mohd Shiraz Aris. "Reacting Flow Characteristics and Multifuel Capabilities of a Multi-Nozzle Dry Low NO_x Combustor: A Numerical Analysis." *CFD Letters* 13, no. 11 (2021): 21-34. https://doi.org/10.37934/cfdl.13.11.2134

[27] Rahman, Mohammad Nurizat, Mohd Shiraz Aris, Mohd Haffis Ujir, and Mohd Hariffin Boosroh. "Predictive Numerical Analysis to Optimize Ventilation Performance in a Hydropower Surge Chamber for H2S Removal." *CFD Letters* 13, no. 10 (2021): 69-80. https://doi.org/10.37934/cfdl.13.10.6980

[28] Rahman, M. N., M. A. Wahid, and MF Mohd Yasin. "Predictive Numerical Analysis on the Fuel Homogeneity in a Rotating Detonation Engine (RDE) Implementing Radially-Entered Fuel Injection Scheme." In *IOP Conference Series: Materials Science and Engineering*, vol. 884, no. 1, p. 012109. IOP Publishing, 2020. https://iopscience.iop.org/article/10.1088/1757-899X/884/1/012109

[29] Mazlan, Muhammad Amri, Mohd Fairus Mohd Yasin, Saat Aminuddin, Mazlan Abdul Wahid, Ahmad Dairobi Ghazali, and Mohammad Nurizat Rahman. "Initiation Characteristics of Rotating Supersonic Combustion Engine." *Evergreen* 8, no. 1 (2021): 177-181. https://doi.org/10.5109/4372275

[30] Rahman, Mohammad Nurizat, Mazlan Abdul Wahid, Mohd Fairus Mohd Yasin, Abidin Ummikalsom, and Muhammad Amri Mazlan. "Predictive Numerical Analysis on the Mixing Characteristics in a Rotating Detonation Engine (RDE)." *Evergreen* 8, no. 1 (2021): 123-130. https://doi.org/10.5109/4372268

[31] Rahman, Mohammad Nurizat, Norshakina Shahril, Suzana Yusup, and Ismail Shariff. "Hydrogen Co-Firing Characteristics in a Single Swirl Burner: A Numerical Analysis." In *IOP Conference Series: Materials Science and Engineering*, vol. 1257, no. 1, p. 012020. IOP Publishing, 2022. https://doi.org/10.1088/1757-899X/1257/1/012020

[32] Shi, Hang, Yuxin Wu, Man Zhang, Yang Zhang, and Junfu Lyu. "Ash deposition of Zhundong coal in a 350 MW pulverized coal furnace: Influence of sulfation." *Fuel* 260 (2020): 116317. https://doi.org/10.1016/j.fuel.2019.116317

[33] Wang, Yongzhen, Jing Jin, Dunyu Liu, Haoran Yang, and Xuesen Kou. "Understanding ash deposition for Zhundong coal combustion in 330 MW utility boiler: Focusing on surface temperature effects." *Fuel* 216 (2018): 697-706. https://doi.org/10.1016/j.fuel.2017.08.112

[34] Cai, Yongtie, Kunlin Tay, Zhimin Zheng, Wenming Yang, Hui Wang, Guang Zeng, Zhiwang Li, Siah Keng Boon, and Prabakaran Subbaiah. "Modeling of ash formation and deposition processes in coal and biomass fired boilers: A comprehensive review." *Applied Energy* 230 (2018): 1447-1544. https://doi.org/10.1016/j.apenergy.2018.08.084

[35] Rahman, Mohammad Nurizat, and Nor Fadzilah Binti Othman. "A numerical model for ash deposition based on actual operating conditions of a 700 MW coal-fired power plant: Validation feedback loop via structural similarity indexes (SSIMs)." *CFD Letters* 14, no. 1 (2022): 99-111. https://doi.org/10.37934/cfdl.14.1.99111

[36] Rahman, Mohammad Nurizat. "Optimisation of Solid Fuel In-furnace Blending for an Opposed-firing Utility Boiler: A Numerical Analysis." *CFD Letters* 14, no. 9 (2022): 89-107. https://doi.org/10.37934/cfdl.14.9.89107

[37] Yang, Joo-Hyang, et al. "Effects of detailed operating parameters on combustion in two 500-MWe coal-fired boilers of an identical design." *Fuel* 144 (2015): 145-156. https://doi.org/10.1016/j.fuel.2014.12.017

[38] Ferziger, Joel H., Milovan Perić, and Robert L. Street. *Computational methods for fluid dynamics*. Vol. 3. Berlin: springer, 2002. https://doi.org/10.1007/978-3-319-99693-6

[39] Sun, Jian, et al. "Numerical investigation of a non-premixed hollow rotating detonation engine." *international journal of hydrogen energy* 44.31 (2019): 17084-17094. https://doi.org/10.1016/j.ijhydene.2019.04.168

[40] Sakuragi, Kiyoshi, and Maromu Otaka. "Effect of biomass carbonization on the grinding of coal/biomass mixtures." *ACS omega* 5, no. 34 (2020): 21722-21727. https://pubs.acs.org/doi/10.1021/acsomega.0c02629#

[41] Du, Lianxiang, Kevin J. Folliard, and David Trejo. "Effects of constituent materials and quantities on water demand and compressive strength of controlled low-strength material." *Journal of materials in Civil Engineering* 14, no. 6 (2002): 485-495. https://doi.org/10.1061/(ASCE)0899-1561(2002)14:6(485)

1.4.3 Sustainable Production of Value-Added Products and Energies from Oil Palm Residues and Plastic Waste Mixtures in the ASEAN Region

Team Members:

1. Bridgid Chin Lai Fui, Department of Chemical and Energy Engineering, Faculty of Engineering and Science, Curtin University Malaysia, Associate Professor, Malaysia

2. Armando T. Quitain, College of Cross-Cultural and Multi Discipline Studies Kumamoto University, Professor, Malaysia

3. Suttichai Assabumrungrat, Bio-Circular-Green-economy Technology & Engineering Center (BCGeTEC), Department of Chemical Engineering, Faculty of Engineering, Chulalongkorn University, Professor, Malaysia

4. Suzana Yusup, Generation Unit (Fuel Technology & Combustion), Tenaga Nasional Berhad (TNB) Research Sdn Bhd, Principal Investigator, Malaysia

5. Hj. Ismail Shariff, Generation Unit (Fuel Technology & Combustion), Tenaga Nasional Berhad (TNB) Research Sdn Bhd, Head of Generation, Malaysia

6. Mohammad Nurizat B. Rahman, Generation Unit (Fuel Technology & Combustion), Tenaga Nasional Berhad (TNB) Research Sdn Bhd, Senior Power Generation Researcher, Malaysia

7. Worapon Kiatkittipong, Department of Chemical Engineering, Faculty of Engineering and Industrial Technology, Silpakorn University, Associate Professor, Thailand

8. Elisabeth Rianawati, Resilience Development Initiative (RDI), Director, Indonesia

9. Yiin Chung Loong, Department of Chemical and Energy Sustainability, Faculty of Engineering, Universiti Malaysia Sarawak (UNIMAS), Lecturer, Malaysia

10. Jonas Karl Agutaya, Graduate School of Science and Technology, Kumamoto University, Postdoctoral Researcher, Japan

11. Atthapon Srifa, Department of Chemical Engineering, Faculty of Engineering, Mahidol University, Assistant Professor, Thailand.

12. Apiluck Eiad-ua, College of Nanotechnology, King Mongkut's Institute of Technology Lakrabang, Assistant Professor, Thailand

13. Neeranuch Phusunti, Department of Chemistry, Faculty of Science, Prince of Songkla University, Associate Professor, Thailand

Abstract

This research project aims to utilize the mixtures of oil palm residues and plastic waste mixtures to convert value-added products and energies. In this research, the hydropyrolysis process had been selected to convert the plastic and palm oil biomass into hydrocarbon oil production. The selected oil palm residue is palm kernel shell and plastic waste is high density polyethylene (HDPE). A simulation work had been conducted using the ASPEN Plus software. This process aims to produce around 100,000 tonnes of bio-oil with a purity of 99%. The process design and techno-economic analyses of hydropyrolysis of oil palm residues and plastic waste mixtures would be presented in this report.

Research Summary

1. Bio-oil is also known as the hydrocarbon oil which can be used for heat generation, power generation, and as a transportation fuel for heavy-duty engines. Palm kernel shell is selected due to its abundance supply among palm oil biomass in ASEAN region, and HDPE is able to cater high volatile content which could increase the bio-oil production efficiency. Fast catalytic hydropyrolysis is an advanced thermochemical conversion that efficiently converts lignocellulosic feedstock into high quality hydrocarbons. Catalyst such as zeolite is introduced into the system to allow the hydrocarbon to broken down into smaller molecules. In addition, a hydrogen will be introduced into the system to stabiles the reactive intermediates formed during the pyrolysisi process and reducing the formation of char and ash.
2. Table 1 shows the proximate and ultimate analyses for both palm oil biomass and HDPE.

Table 1
Proximate and ultimate analysis.

Proximate analysis (wt% wet basis)	PKS	HDPE	Ultimate analysis (wt.% dry basis)	PKS	HDPE
Moisture content	12.00	0.00	C	49.23	85.71
Volatile matter	30.53	99.67	H	5.04	14.29
Fixed carbon	48.50	0.00	O	44.94	0.00
Ash	8.97	0.33	N	0.74	0.00
Holocellulose	54.30	–	S	0.05	0.00
Alpha-cellulose	29.60	–	Density (kg/m^3)	733	1194
Lignin	59.30	–	HHV (MJ/kg)	24.97	45.98

3. The ASPEN Plus Process Simulation Flowsheet for hydropyrolysis of oil palm residue and plastic waste mixture is shown in Figure 1.

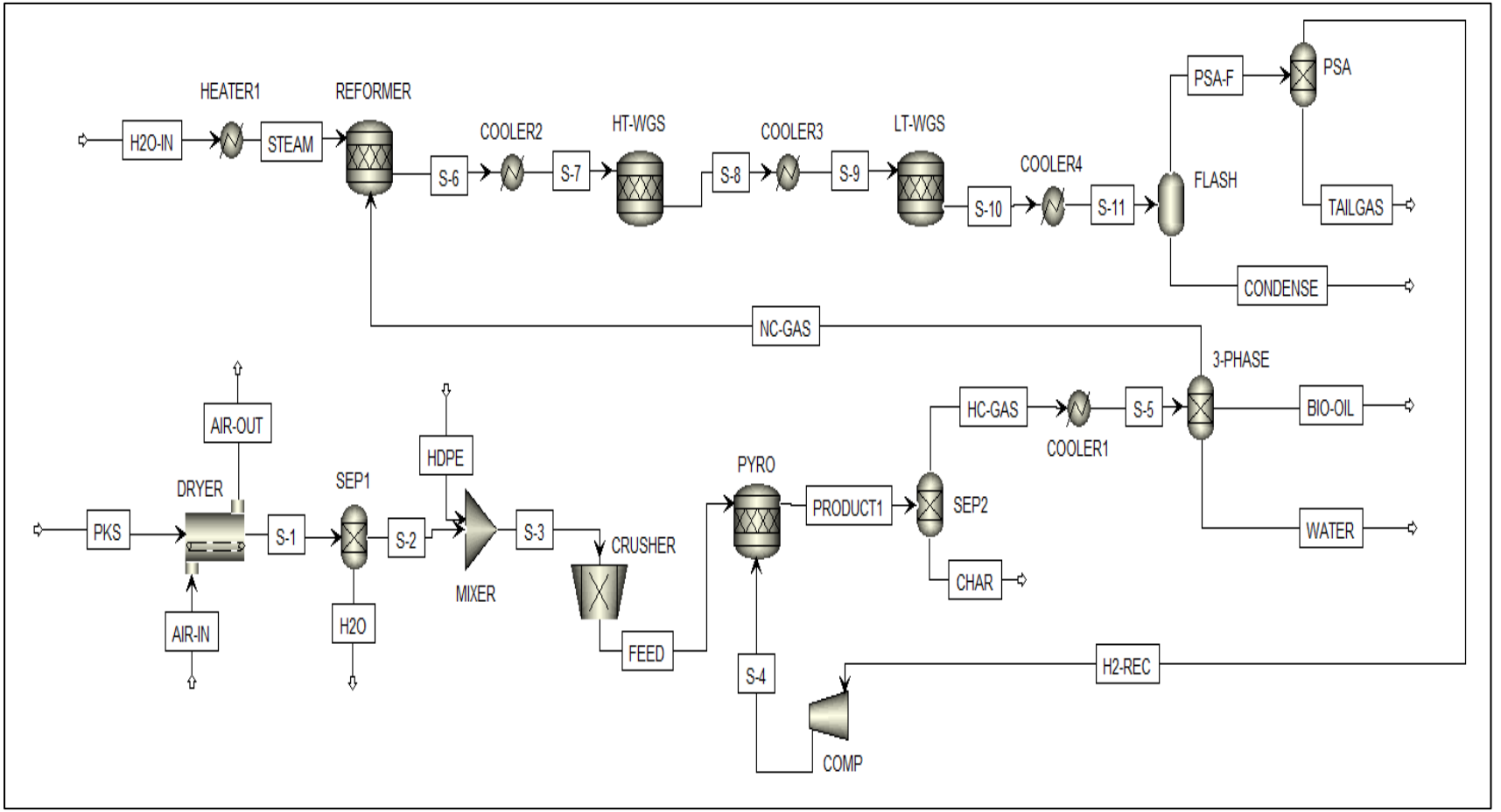

Figure 1: Aspen Plus Process Simulation Flowsheet for hydropyrolysis of oil palm residue and plastic waste mixture

Equipment Label	Type of Equipment	Specifications
D-301	Flash drum	T = 40°C, P = 15 bar
E-101	Dryer	Length = 10 m, Solid residence time = 1.5 hours Counter-current air flow: T = 200°C, P = 1 bar, Total flow rate = 280 tonne/day
E-102	Pre-heater	T = 300°C, P = 1 bar
E-201	Condenser	T = 70°C, P = 50 bar
E-301	Water heater	T = 100°C, Vapor fraction = 1
E-302	Cooler	T = 350°C, P = 1 bar
E-303	Cooler	T = 250°C, P = 16 bar
E-304	Cooler	T = 40°C, P = 15 bar
JC-301	Compressor	Type: Isentropic, Discharge pressure: 50 bar
M-101	Mixer	Parameters not specified.
R-201	Fast catalytic hydropyrolysis reactor	Type: RStoic T = 500°C, P = 30 bar **Reactions:** Cellulose: $4C_6H_{10}O_5 + 15H_2 \rightarrow 9CH_4 + C_8H_{18} + 5CO_2 + 2CO + 8H_2O$ Hemicellulose: $10C_5H_8O_4 + 37H_2 \rightarrow C_4H_8 + C_7H_{16} + C_{12}H_{26} + C_{19}H_{40} + 8CO + 3H_2O$ Lignin: $3C_{15}H_{14}O_4 + 3H_2 \rightarrow 2CH_4 + 2C_2H_4 + C_6H_6 + 2C_7H_8 + C_{10}H_8 + 3CO_2 + 5CO + H_2O + C$ HDPE: $2(C_2H_4)_n + 3H_2 \rightarrow 2CH_4 + C_2H_6$ The fractional conversion for all reactions above is 0.98, assuming that the presence of zeolite catalyst leads to higher rate of chemical reactions.
R-301	Steam reforming reactor	Type: RStoic T = 700°C, P = 10 bar **Reactions:** $CH_4 + H_2O \rightarrow CO + 3H_2O$ $C_2H_4 + 2H_2O \rightarrow 2CO + 4H_2$ $C_2H_6 + 2H_2O \rightarrow 2CO + 5H_2$ $C_4H_8 + 4H_2O \rightarrow 4CO + 8H_2$ The fractional conversion for all reactions above is 0.95.

R-302	High-temperature water-gas shift	Type: RStoic P = 15 bar, Duty = 0 kW **Reaction:** $CO + H_2O \rightarrow CO_2 + H_2$ Fractional conversion of CO = 0.95
R-303	Low-temperature water-gas shift	Type: RStoic P = 15 bar, Duty = 0 kW **Reaction:** $CO + H_2O \rightarrow CO_2 + H_2$ Fractional conversion of CO = 0.95
SR-101	Crusher	Crusher type: Gyratory, Selection and breakage function: US Bureau of Mines, Maximum particle diameter: 0.002 m
V-101	Vapour-solid separator	All water is separated from the stream; Split fraction of water = 1
V-201	Gas-solid separator	All solids are removed from the stream as biochar; Split fraction of solids (C, cellulose, hemicellulose, lignin and HDPE) = 0.999, assuming that small amount of solid particles remained in the stream.
V-202	Three-phase separator	S-5 stream are separated into non-condensable gases (NC-GAS), bio-oil (BIO-OIL) and water (WATER). $C_2 - C_5$ light hydrocarbons are split into NC-GAS stream, while heavy hydrocarbons (C_6 and above) are split into BIO-OIL stream. NC-GAS: Split fraction of H_2, CO_2, CO, CH_4, C_2H_4, C_4H_8, O_2, N_2 = 1 BIO-OIL: Other components are split into this stream. WATER: Split fraction of water = 1
V-301	Pressure swing adsorption (PSA) unit	Split fraction of H_2 = 0.9; other gases are removed in TAILGAS stream.

The purchased equipment with installation costs USD 14,059,043.35 meanwhile the fixed capital investment (FCI) is USD83,743,788.58. The total capital investment (TCI) amounts to USD 98,482,695.37 after considering the working capital and Southeast Asia location factor of 1.12. Variable Costs of Production (VCOP) include raw materials: palm kernel shell (PKS), high-density polyethylene (HDPE), zeolite (ZSM-5) catalyst, and hydrogen gas for the first process (one-time purchase), with the packaging costs of products. Fixed Costs of Production (FCOP) include operating labour and supervisory wages, utilities, maintenance and repairs, operating supplies, laboratory charges, patents and royalties, property taxes and insurance, direct salary overhead, general plant overhead, financing, environmental charges and security. General expenses include administrative, distribution, marketing, and research and development (R&D) costs. The total cost of production (operating costs) estimated is USD 65,008,434,66.

Table 2: Total Capital Investment (TCI) of the plant.

	Description	Cost ($/USD)
Direct Cost		
Purchased Equipment, E	Obtained from **Table 1**.	14,059,043.35
Delivery of Purchased Equipment	Expenses for shipping and locating purchased equipment to the site; 10% E (Towler and Sinnott 2020).	1,405,904.33
Purchased Equipment Installation	Cost of setting up and installing the equipment at the site; 39% E (Towler and Sinnott 2020).	5,623,617.34
Yard Improvement	Costs associated with site preparation, such as land grading or infrastructure enhancements; 20% E (Towler and Sinnott 2020).	2,811,808.67
Service Facilities	Costs for additional services like electrical, water, and gas connections for equipment; 60% E (Towler and Sinnott 2020).	8,435,426.01
Total Direct Cost (D)		**32,335,799.69**
Indirect Cost		
Engineering and Supervision	Costs for engineering design, supervision, and management during the construction and installation phase; 30% E (Towler and Sinnott 2020).	4,217,713.00
Construction Expenses	Miscellaneous construction-related costs; 15% D (Towler and Sinnott 2020)	4,850,369.95
Total Indirect Cost (I)		**9,068,082.96**
Total Direct and Indirect Cost (D + I)		**41,403,882.65**
Contractor's Fee	Payment made to project contractors; 10% (D + I) (Towler and Sinnott 2020).	4,140,388.27
Contingency	A reserved fund for unforeseen expenses; 25% (D + I) (Towler and Sinnott 2020).	10,350,970.66
Land	Land area: 2.186×10^6 ft^2; price of purchase: \$12.74/ft^2 (Memo 1)	27,848,547.00
Fixed Capital Investment (FCI)		**83,743,788.58**
Working Capital	Additional funds required to cover initial operating expenses, beyond the cost of building the plant, to initiate operations (start-up) and sustain them until the plant begins earning income; 5% FCI (Towler and Sinnott 2020).	4,187,189.43
Total Capital Investment (TCI)		**87,930,978.01**
TCI Considering Location Factor (SE Asia)	The location factor of Southeast Asia countries is 1.12 (Towler and Sinnott 2020).	**98,482,695.37**

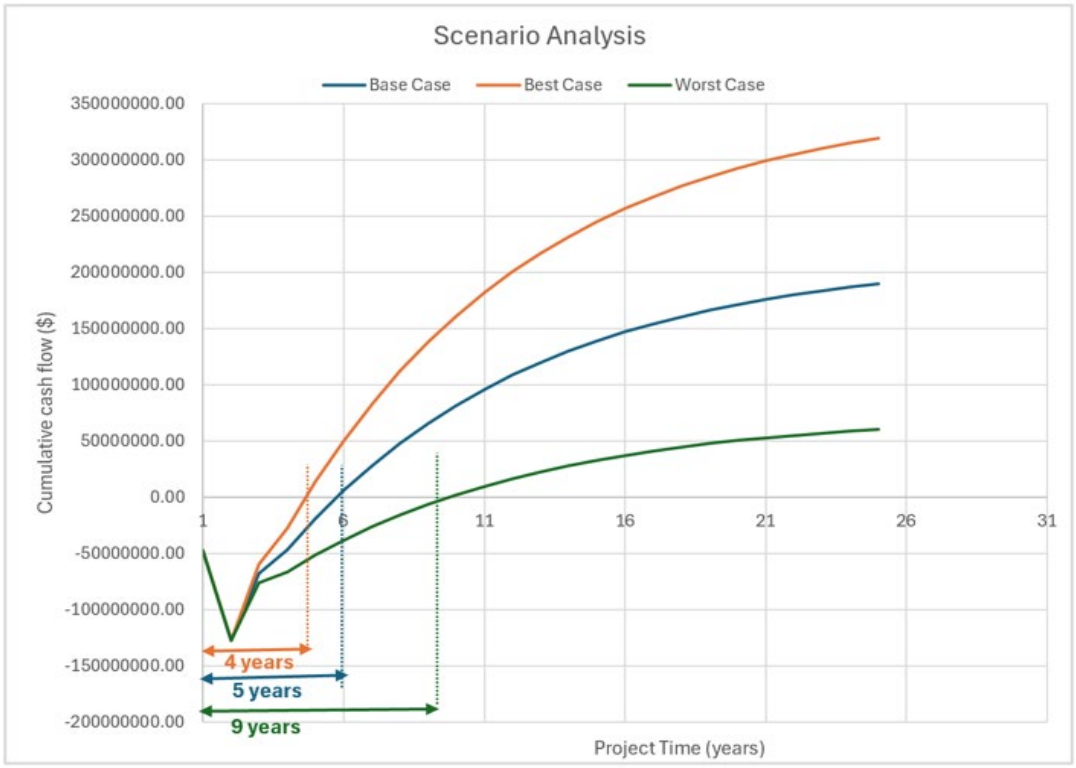

Figure 2: Scenario analysis for the base, best, and worst-case scenarios

Table 3: Details of the cumulative net profit and return on investment for the base, best, and worst case scenarios.

Case	Cumulative Net Profit ($)	Return on Investment (%)
Base	984640717.78	47.03
Best (+20%)	1494293350.29	71.37
Worst (-20%)	474988085.27	22.69

4. From **Table 4**, it is found that the plant aligns with the United Nations Sustainable Development Goals (SDGs), achieving a total score of 126/170, along with their justifications. This score reflects the plant's to a more sustainable future in environmental and socio-economic contexts.

Table 4: Evaluation of plant based on the Sustainable Development Goals.

No. of SDG	Sustainable Development Goal(s)	Score (/10)	Justifications
1	No Poverty	8	The plant can employ unskilled labour in feedstock collection, processing, and plant operations. The average salary of an unskilled worker ranges from RM1,500 to RM2,500, while the average salary of a plant operator in Malaysia ranges from RM 2,380 to RM 7,570 per month (Aurawoo 2024; SalaryExpert 2024). Also, it could boost farmers' income by supplying palm kernel shells.
2	Zero Hunger	5	Workers' employment can improve food security and nutrition. In Bintulu, the average monthly expenses of a family are approximately USD 250 (Traveltable 2023). Biochar produced as a byproduct can be used as fertilizers to enhance soil quality, indirectly promoting sustainable agriculture and food security.
3	Good Health and Well-Being	6	The plant has implemented air pollution control technologies such as filters to reduce volatile organic compounds (VOCs) and particulates from the hydropyrolysis process. The process emits fewer harmful pollutants than traditional pyrolysis, ensuring personnel's healthy lives. Integrating hydropyrolysis with recycled HDPE reduces ash production and decreases plastic waste. Reusing hydrogen gas and selling biochar reduces waste from plants and promotes well-being.
4	Quality Education	7	Educational programs, technical training, and upskilling opportunities provided by the plant to its employees and local communities can contribute to improving local educational standards. These initiatives also help employees to improve their skills and knowledge, contributing to a better-educated workforce in the community.
5	Gender Equality	6	The plant can establish policies to promote gender equality in hiring, equal pay, and leadership opportunities to promote equal employment opportunities for women in technical and non-technical roles. This can be enhanced through partnerships with women empowerment organizations or government schemes.
6	Clean Water and Sanitation	8	The wastewater produced from the process undergoes treatment for reuse to minimize water withdrawal and ensure the wastewater is safe for environmental discharge (based on government standards). No harmful chemicals are discharged into water bodies, ensuring the protection of local water resources.
7	Affordable and Clean Energy	10	The bio-oil produced can be used in local industries as a substitute for diesel. The plant can also integrate solar power for auxiliary systems.
8	Decent Work and Economic Growth	8	The plant has created numerous jobs in the local community, employing both skilled and unskilled workers. Fair wages are ensured, and labour conditions comply with national labour laws. This can contribute to local economic growth.
9	Industry, Innovation, and Infrastructure	9	The plant has adopted the fast catalytic hydro pyrolysis process, which significantly improves the conversion efficiency of PKS and HDPE to bio-oil and biochar. This method is new and innovative in terms of technology and infrastructure development. Automation and remote monitoring systems can improve the plant's performance and resilience.
10	Reduced Inequalities	6	The plant aims to make an effort to hire from disadvantaged and marginalized groups, including rural labourers and people with limited access to formal education. Offering equitable pay and promoting employees from these communities reduces regional inequalities.
11	Sustainable Cities and Communities	9	The plant directly reduces plastic pollution in nearby urban areas by recycling HDPE plastic waste into valuable products. Bio-oil provides high-quality green and sustainable fuel to local industries or aviation fields, while biochar helps in soil restoration efforts.
12	Responsible Consumption and Production	8	The plant operates on the principles of a circular economy, converting waste materials (PKS and recycled HDPE) into valuable waste products like bio-oil and biochar. Using waste as a feedstock, the plant promotes responsible production and reduces dependency on virgin materials. In addition, the plant minimizes waste generation during production through efficiency optimizations.
13	Climate Action	7	The plant produces bio-oil as a sustainable fuel alternative, which can reduce carbon emissions from traditional fossil fuels.
14	Life Below Water	6	Treating the wastewater before discharging can protect marine ecosystems and prevent pollution of oceans, seas, and marine resources.
15	Life on Land	8	The plant is located in an industrial area, which will not affect the terrestrial ecosystems and will not lead to any deforestation activities.
16	Peace, Justice, and Strong Institutions	7	The plant is designed with a strong governance structure that promotes transparency, ethical business practices, and accountability. It complies with environmental and labour laws, ensuring workers' rights and building strong institutional frameworks.
17	Partnerships for the Goals	8	The plant partners with research institutions and government agencies to improve hydropyrolysis technologies and promote sustainable waste management practices. This promotes knowledge sharing and increases access to funding and expertise.
Total score (/170)		**126**	

Publication List:

Conference Paper

1. S.K.Y. Yap, B.L.F. Chin, C.L. Yiin, S. Yusup, A.T. Quitain, S.Assabumrungrat, E. Rianawati, Synergistic Effects on the Catalytic Co-Pyrolysis of Palm Kernel Shell Waste and Tetra Pak Mixtures via Thermogravimetric Approach. 2nd International Conference on Tropical Sciences: Harmonising Nature with Humanity (TropSc 2024), 16-17 October 2024, Kuching Malaysia. ***(Just accepted)***

Journal

1. Chee, A.L.K., Chin, B.L.F., Goh, S.M.X., Chai, Y.H., Loy, A.C.M., Cheah, K.W., Yiin, C.L., Lock, S.S.M., 2023. Thermo-catalytic co-pyrolysis of palm kernel shell and plastic waste mixtures using bifunctional HZSM-5/limestone catalyst: kinetic and thermodynamic insights. Journal of the Energy Institute 107, 101194. https://doi.org/10.1016/j.joei.2023.101194
2. Chang, K.J., Loy, A.C.M., Chin, B.L.F., Alhamzi, H., Lam, M.K., How, B.S., Yusup, S., Yiin, C.L., Quitain, A.T., Assabumrungrat, S., Rianawati, E., n.d. Parametric Analysis and Techno-Economic Analyses of Transforming Palm Oil Wastes to Biofuel *via* Thermochemical Methods: An ASPEN Plus modelling Study, Energy ***(Under Review)***
3. Wee, M.X.J., Chin, B.L.F., Saptoro, A., Chew, J.J., Sunarso, J., Yusup, S., Sharma, A., Catalytic co-pyrolysis of oil palm empty fruit bunches (EFB) and surgical face mask (SFM): themo-kinetic study, ANN model fitting and synergistic effect. Journal of the Taiwan Institute of Chemical Engineers (***Under Review)***

Group Workshops, Meetings, and Research Exchange

9th JASTIP-WP2 Annual Workshop on the 26th January 2024 at National Science and Technology Development Agency (NSTDA), Bangkok Thailand.

2.1 Development of New Functional Materials for Energy and Environment

Researchers

1. Prof. Keiichi N Ishihara, Kyoto University
2. Prof. Hideyuki Okumura, Kyoto University
3. Prof. Wisanu Pecharapa, King Mongkut's Institute of Technology Ladkrabang
4. Prof. Sorapong Pavasupree, Rajamangala University of Technology Thanyaburi

Our group have developed the functional materials that can be applied in energy and environment applications. Er/Yb-doped $BiVO_4$ photocatalyst has been prepared by sonochemical process and the prepared product exhibits the photocatalytic performance under infrared irradiation due to photon up-conversion phenomena. Rare-earth/Al co-doped CuS powders with good infrared absorption property can be prepared in large scale production by facile co-precipitation method. Ball milling process was employed to synthesize M_xWO_3 (M=Na,K)material for infrared shielding for energy conservation applications. Hydrothermal process was used to prepare NH_4WO_3 material that could be applied as infrared active materials in energy applications. SiO_2/TiO_2 based composite prepared by sonochemical process could be utilized for self-cleaning application.

Research Summary

Er/Yb co-doping effectively enhances the infrared-driven photocatalytic performance of $BiVO_4$ nanoparticles. Phase transformation from monoclinic to tetragonal $BiVO_4$ and significant up-conversion process induced by Yb and Er ions are key mechanisms for this improvement. the facile synthesis of CuS particle via co-precipitation method. The influence of Al and Yb ions as the potential dopants on structural and optical properties of CuS are investigated. It is found that both Al and Yb dopants have significant influence on the optical properties, especially in NIR spectra region. Al dopant could enhance the LSPR-induced NIR absorptivity of CuS while Yb dopant could further increase the NIR absorption due to characteristic transition of Yb ions. Sodium tungsten bronze particles was prepared using the high-energy ball milling method, optimized for a milling time of 2.5 hours. The resulting crystal structure revealed the presence of pure $Na_{0.3}WO_3$ achieved without additional of annealing processes. The milling time, played a significant role for reducing the oxidation number of W^{6+} to W^{5+} oxidation states, thereby enhancing the Near Infrared (NIR) shielding performance. The synthesis of CuO-TiO_2-SiO_2

nanocomposites with different Cu precursor loading was achieved by a sonochemical process. the compositions of CuO-TiO_2-SiO_2 nanocomposites with different Cu precursor loading indicates the increase of TiO_2 phase with a high Cu precursor corresponding to the diminishing SiO_2 phase. The high efficiency of the antibacterial property of CuO-TiO_2-SiO_2 nanocomposite can be obtained at 0.5 wt.%Cu precursor with thoroughly covering CuO clusters on the TiO_2-SiO_2 composite.

Year: 2023 (Sept 2022-Aug 2023)

Publications

1. Thanaphon Kansaard, Keiichi N Ishihara, Wisanu Pecharapa, "Characterization and Visible Light-driven Photocatalytic Activity of $BiVO_4$/BiOCl/Bi_2S_3 Nanocomposites Prepared by Sonochemical Process", Physica Status Solidi: A (Applications and Materials Science), 2023, 220, Article Number 2200447.
2. Maneerat Songpanit, Kanokthip Boonyarattanakalin, Saksorn Limwichean, Tossaporn Lertvanithphol, Mati Horprathum, Wisanu Pecharapa, Wanichaya Mekprasart, "Structural and Optical Characterizations of Polymethyl Methacrylate Films with the Incorporation of Ultrafine SiO_2/TiO_2 Composite Utilized as Self-cleaning Surfaces" Polymers, 2023, 15(15), 3162 DOI: 10.3390/polym15153162.
3. Kanokthip Boonyarattanakalin, Tanisara Noinonmueng, Thanaphon Kansaard, Wanichaya Mekprasart, Tirapat Wechprasit and Wisanu Pecharapa, "Influence of Yb ion dopant on Physical, Optical and Photocatalytic Properties of Er-doped $BiVO_4$ Synthesized by One-step Sonochemical Process, Integrated Ferroelectrics, 2023, 239, 94-103 DOI:10.1080/10584587.2023.2234613.
4. Natchapon Rattanaanothaikul, Parituch Lattanand, Maneerat Songpanit, Sutee Chutipaijit, Wanichaya Mekprasart, "The influence of plastic wrap types on oxygen detection property by colorimetric oxygen indicator based on TiO_2/methylene blue nanocomposite", Thai Journal of Nanoscience and Nanotechnology, 2023, 8(2), 10-18.
5. Maneerat Songpanit, Saksorn Limwichean, Mati Horprathum, Wanichaya Mekprasart, Wisanu Pecharapa, "The Addition of TiO_2 Ratios in SiO_2–TiO_2 Nanocomposite by Sonochemical Process for the Enhancement in Self-cleaning Property", IOP Conf. Series: Materials Science and Engineering, 2023, 1286, 012005
6. Maneerat Songpanit, Kanokthip Boonyarattanakalin, Saksorn Limwichean, Tossaporn Lertvanithphol, Mati Horprathum, Wisanu Pecharapa, Wanichaya Mekprasart, "Self-cleaning SiO_2/TiO_2/PMMA nanocomposite films fabricated by spin coating technique: Effect

of different spin speed and film layers", Journal of Materials Science and Applied Energy, 2023, 12(3), 252043

Presentations

- "Nanomaterials with surface plasmon resonance property for optical applications", the 15th Eco-Energy and Materials Science and Engineering Symposium (EMSES2022), 7-10 December 2022 Dusit Thani Pattaya, Chonburi, Thailand.

- "Effect of Er ion on Physical, Optical and Low-photon-energy Driven Photocatalytic Properties of Yb-doped $BiVO_4$ Synthesized by One-step Sonochemical Process", The 4 th of Materials Research Society of Thailand International Conference (MRS-Thailand 2023), 28 February – 4 March 2023, Sunee Grand Hotel & Convention Center, Ubon Ratchathani, Thailand.

- "Self-cleaning SiO_2/TiO_2/PMMA nanocomposite films fabricated by spin coating technique: effect of different spinning speed and film layers", The 4 th of Materials Research Society of Thailand International Conference (MRS-Thailand 2023), 28 February – 4 March 2023, Sunee Grand Hotel & Convention Center, Ubon Ratchathani, Thailand.

- "Low-dimensional structured materials for optical harvesting and management", 18th Siam Physics Congress (SPC2023), 14-16 June 2023, Empress Convention Centre, Chiang Mai, Thailand.

Researchers

1. Prof. Hideaki Ohgaki	Kyoto University
2. Assit Prof. Jordi Cravioto C.	Kyoto University
3. Prof. Nasrudin Abd Rahim	University of Malaya
4. Sen. Lect. Tan Chia Kwang	University of Malaya
5. Sen. Lect. Hang Seng Che	University of Malaya
6. Mr. Anugerah Yuka Asmara	BRIN
7. Dr. Bun Long	Institute of Technology of Cambodia
8. Dr. Vai Vannak	Institute of Technology of Cambodia

Abstract

The sub-unit focuses on socio-environmental issues of energy use in Southeast Asia, combining quantitative and qualitative data approaches. In FY2023, the investigation assessed electricity access impacts on quality of life (QoL) through a mixed methods approach using qualitative data from interviews and visual ethnography conducted in rural communities in Southeast Asia. The study has developed a more detailed understanding of electrification's impact on quality of life and other community issues in rural areas in Malaysia, the Philippines, and, most recently, Indonesia.

RESULTS

In FY2023, we adopted a mixed-methods approach to elaborate a more detailed understanding of the electrification impacts on QoL of beneficiaries in the rural communities we have been working within Malaysia, the Philippines and Indonesia, and the resulting community disparities from the electrification process.

We conducted 92 semi-structured interviews with community members (32 in Malaysia, 10 in the Philippines, 50 in Indonesia), four interviews with stakeholders (The Philippines) and one focus group (The Philippines). We also recorded audio-visual material for visual ethnographies of households and activities in rural communities receiving electricity access.

The analysis of the collected information is still in progress, and the emerging results from these analyses have been presented in various forums for discussion. One example is our research presentation at the Energy Resources and the Environment section of the European Geosciences General Assembly in April 2023, where we discussed how relevant circular economy visions are in the context of rural communities that lack electrification and receive access through solar PV technologies. Our work emphasised some problems we identified through our analyses, such as malfunction and short life of PV systems delivered in the communities and the waste generation from early end-of-life of such systems.

Another example was a comparative analysis of electrification effects on quality of life in Malaysia and The Philippines, presented at the 6th International Conference on Clean Energy and Technology in Penang, Malaysia. We demonstrated how demographic profiles can determine significant differences in the effects of electrification on the quality of life of community members. Several other invited lectures in Indonesia and Japan also allowed receiving feedback on this and more recent findings from our comparative analyses.

In addition, with our colleagues from BRIN Indonesia, we published an article about the governance of sustainable photovoltaic innovation systems, where we identified issues related to unsustainable PV projects in Indonesia (e.g., short-life infrastructure, maintenance difficulties) and how stakeholder collaboration could improve them.

Finally, we organised one international workshop, where we successfully discussed the socio-economic impact of renewable energy (solar PV) in rural communities in the region, fieldwork experiences, and the challenges for advancing access to such communities.

In sum, we have advanced the understanding of electrification's impact on quality of life and other community issues, such as disparities and solar PV waste problems in rural Malaysia, the Philippines, and Indonesia.

Publications

1.1 Anugerah Yuka Asmara, AR. Rohman Taufiq Hidayat, B. Kurniawan, H. Ohgaki, T. Mitsufuji, J. Cravioto, Building a Sustainable Photovoltaic Innovation System in Indonesia Through Network Governance Perspective, Environment & Policy, Environmental Governance in Indonesia, 61, 463-485, 2023

1.2 S. Deeum,T. Charoenchan, N. Janjamraj, S. Rompho-chai, S. Baum, H. Ohgaki, N. Mithulananthan, K. Bhumkittipich, Optimal Placement of Electric Vehicle Charging Stations in an Active Distribution Grid with Photovoltaic and Battery Energy Storage System In-tegration, Energies, 16,22, 7628、2023

1.3 S. Basu, K. Usher, H. Tamiya, R. Akasegawa, Y. Hui, Q. Chen, J. Cravioto, H. Ohgaki, Synergies and Trade-offs Quantification from Regional Waste Policy to Sustainable Development Goals: The Case of Kyoto City, Sustainable Development, 1-21, 2024

1.4 D.I. Avila-Ortega, S. Garcidueñas-Nieto, D. Moran, S. Cornell, J. Cravioto, P. Søgaard Jørgensen, C. Flo-res-Santana, R. García Ochoa, G. Engström, Mexico's carbon inequality: Why income matters. Journal of Ecological Economics, ECOLEC-D-23-01421 (under review), 2024

1.5

Presentations

2.1 H. Ohgaki, Roles of Relevant Stakeholders in the National Innovation System, The 1 st National Science Technology Innovation Day, Koh Pich Convention & Exhibition Center, 2023.3.27

2.2 J. Cravioto, H. Ohgaki, C.K. Tan, H.S. Che, Electrification effects on quality of life in Southeast Asia: A comparison of narratives in Malaysia and The Philippines, 6th International Conference on Clean Energy and Technology 2023, Penang, Malaysia, 2023.6

2.3 M. Pal, Q.M.B. Soesanto, S. Zhang, J. Fu, H. Ma, M.H. Imaduddin, J. Cravioto, H. Ohgaki, C. Qu, EV Transition: Consideration of Local Socio-Environmental Impacts from Mining and Recycling, The 14th Inter-national Symposium of Advanced Energy Science, Kyoto University, 2023.8.30-31

2.4 H. Ohgaki, Current Global Energy Situation and Carbon Neutral 2050, Five Day International Faculty Development Program, "EMERGING TECHNOLOGIES IN THERMAL ENERGY PRODUCTION AND STORAGE", Vishnu Educational Development and Innovation Center (VEDIC), Hyderabad, INDIA, 2023.9.15

2.5 H. Ohgaki, ASEAN's Energy Outlook, 2023 International Conference on Power, Energy and Innovation (ICPEI), Amari Hotel, HuaHin, Thailand, 2023.10.19

2.6 J. Cravioto, Gauging the social effects of renewable energy transitions in rural SE Asia, Virtual international Lecture: selected classes on policy analysis. Faculty of Engineering, University of Brawijaya, Indonesia, 2023.10.24

2.7 J. Cravioto, Renewable energy transition: Status, challenges and policy considerations. Virtual seminar on renewable energy utilization policy to reduce the impact of climate change, Faculty of Administrative Science, University of Brawijaya, Indonesia, 2023.10.25
2.8 J. Cravioto, Sustainable transitions, social vulnerabilities and use of energy in the residential sector, Lectures on sustainable urban energy planning, Faculty of Administrative Science, University of Brawijaya, Indonesia, 2023.10.25
2.9 J. Cravioto, H. Ohgaki, Rural Electrification and Quality of Life: Microsociological assessment in the ASEAN region, International Workshop on "Socio-economic impact of renewable energy on communities / issues and policies of solar energy policy to support the Indonesian long-term development planning 2025-2045", School of Industrial and System Engineering, Telkom University, Bandung, Indonesia, 2023.12.8
2.10 H. Ohgaki, Introduction of JASTIP, International Workshop on "Socio-economic impact of renewable energy on communities / issues and policies of solar energy policy to support the Indonesian long-term development planning 2025-2045", School of Industrial and System Engineering, Telkom University, Bandung, Indonesia, 2023.12.8
2.11 J. Cravioto, H. Ohgaki, Rural electrification and QoI: Microsociological assessments in the Southeast Asian region, International Seminar on “Socio Economic Impact of Renewable Energy on Communities” in Cooperation with “Analysing issues and Challenges of Solar Energy Policy to Support the Indonesian Long-Term Development Planning 2025-2045”, Telkom University, Bandung, Indonesia, 2023.12.8
2.12 Sanda Ny Aina Andriamanalina Rakotondramanana, J Cravioto Caballero, H. Ohgaki, Hery tiana Rakotondramiarana, Design Study of Concentrate PV System in an Off-grid Village in the High Plateau of Antananarivo, 4th International Joint Conference of Innovative Africa: Educational Networking Programs for Human Resource Development in Africa’s SDGs, Kyoto University Inamori Building Large Conference Room, 2023.12.18
2.13 J. Cravioto, Solar electrification and Quality of Life in rural Philippines: Mixed-research perspectives, Shiga Prefectural ZeZe High School, 2024.1.14
2.14 M. Pal, Q.M.B. Soesanto, S. Zhang, J. Fu, H. Ma, M.H. Imaduddin, J. Cravioto, H. Ohgaki, C. Qu, Policy Comparison between China and Indonesia on Nickel Mining and Battery Recycling, The 8th Zhejiang-Kyoto-Ajou Joint Symposium on Energy Science, Hangzhou, China, 2024.1.22
2.15 H. Ohgaki, WP2 Activity, The 9th JASTIP-WP2 Annual Workshop, SD202, building no. 12, TSP, NSTDA, 2024.1.26
2.16 H. Ohgaki, J. Cravioto, RE Implementation: Study on Rural Electrification in ASEAN, The 9th JA-STIP-WP2 Annual Workshop, SD202, building no. 12, TSP, NSTDA, 2024.1.26
2.17 J. Cravioto, How does solar energy electrification affect the quality of life?, A micro-sociological view from SE Asia, Shiga Prefectural ZeZe High School 2024.1.27
2.18 J. Cravioto, Developing Research Projects in Social and Interdisciplinary Research Fields, Social Research Guest Lecture, UPN “Veteran” Jawa Timur. Surabaya, Indonesia, 2024.3.8

Workshop
International Workshop on "Socio-economic impact of renewable energy on communities / issues and policies of solar energy policy to support the Indonesian long-term development planning 2025-2045", School of Industrial and System Engineering, Telkom University, Bandung, Indonesia, 2023.12.8